

Stress balances of ice streams in a vertically integrated, higher-order formulation

T.M. KYRKE-SMITH,¹ R.F. KATZ,¹ A.C. FOWLER^{2,3}

¹*Department of Earth Sciences, University of Oxford, Oxford, UK*
E-mail: teresa.kyrke-smith@earth.ox.ac.uk

²*MACSI, Department of Mathematics and Statistics, University of Limerick, Limerick, Republic of Ireland*

³*OCIAM, Mathematical Institute, University of Oxford, Oxford, UK*

ABSTRACT. One challenge in improving our understanding of ice-stream dynamics is to develop models of the spatial and temporal transition from ice-sheet to ice-stream flow. We address this with a new, vertically integrated, higher-order formulation for ice-sheet dynamics that captures the leading-order physics of low aspect ratio, viscous fluid flow, regardless of the amount of slip at the bed. The theory introduces a parameter, λ , which approximates the ratio of the basal stress to the shear stress scale, providing a measure of the relative importance of sliding and internal deformation. Our model is able to simultaneously describe the dynamics of both a slow-moving sheet and rapidly flowing ice streams. To test the formulation, we apply a triple-valued sliding law as the basal boundary condition and obtain numerical solutions that can be compared with previous work. We investigate the sensitivity of flow regimes and shear margin width to parameter variation, deriving a scaling for the latter. We also consider a double-valued sliding law, which enforces a constant, low basal stress beneath the ice stream. Comparisons of the resultant stress fields illustrate the different stress balances that can maintain ice-stream flow.

1. INTRODUCTION

An ice stream is a region of an inland ice sheet where the ice flows much more rapidly than the surrounding ice (Swithinbank, 1954). The reasons for the existence of some ice streams is clear; variations in bedrock topography cause ice to be channelled into bedrock troughs. The thicker ice then leads to larger shear stresses and hence faster flow (e.g. Rutford Ice Stream, West Antarctica (Doake and others, 2001); Jakobshavn Isbræ, Greenland (Clarke and Echelmeyer, 1996)). This is the same concept as for an outlet glacier, except that for a common outlet glacier one expects the bedrock walls of the topographic low to be exposed (Truffer and Echelmeyer, 2003). As Swithinbank (1954) pointed out, there exist some ice streams draining an ice-sheet basin that do not appear to have bedrock highs defining their margins. These are known as pure ice streams; the most prominent examples being the five distinct streams flowing out to the Ross Ice Shelf in the Siple Coast region of Antarctica (Shabtaie and Bentley, 1987; Paterson, 1994; Joughin and Tulaczyk, 2002; Bennett, 2003). Shear zones mark their boundaries and these margins are often highly crevassed due to the horizontal shear stresses exceeding the tensile strength of the ice (Echelmeyer and others, 1994; Bindschadler and others, 2001; Raymond and others, 2001). It appears that in these fast-moving streams basal sliding is a dominant component of the motion, driven by the presence of meltwater or deformable wet sediment slurries at the base of the sheet (Alley and others, 1987; Clarke, 2005; Lemke and others, 2007). There are, however, many questions about these processes yet to be answered, because the bed of an ice sheet is a relatively inaccessible environment, and because the physics governing the coupled behaviour of the ice with meltwater drainage through the bed is a relatively underdeveloped area of research.

Ice streams are an important phenomenon to understand, since a significant proportion of all ice and sediment

discharge occurs through them, despite the fact that they are only found over a small proportion of an ice sheet. In Antarctica, for example, it is estimated that ice streams cover ~10% of the ice sheet's surface, but transmit up to 90% of drainage (Bamber and others, 2000; Rignot and others, 2011). It is therefore vital to learn more about their behaviour, both to help in understanding past ice-sheet collapse, and to predict the evolution of current ice sheets into the future.

A significant challenge in ice-sheet dynamics is to accurately capture the transition from ice-sheet to ice-stream flow; this is critically important in modelling the temporal emergence and stagnation of ice streams. While most of an ice sheet is frozen to the bed, resulting in gravity-driven vertical shear, in ice streams the ice slips over the bed, introducing significant membrane stress gradients. An appropriate model must be able to describe both types of behaviour; under the assumption that ice is an incompressible viscous fluid, the Stokes equation provides a suitable description of all flow regimes. However, these equations are computationally expensive to solve in three dimensions (3-D) and approximations are commonly used. Two such approximations, representing end-member models, are the shallow-ice approximation (SIA; Fowler and Larson, 1978; Morland and Johnson, 1980; Hutter, 1983) and shallow-shelf approximation (SSA; MacAyeal, 1989; Weis and others, 1999). The SIA assumes that the ice is frozen to the bed or only slipping very slowly; vertical shear stresses are supported by the basal drag in the stress balance. The approximation is valid only in regions of low basal slip, and its accuracy decreases significantly as the amount of basal slip increases (Gudmundsson, 2003; Hindmarsh, 2004). The SSA assumes there are no basal shear stresses and horizontal velocities therefore do not vary with depth. It can accurately describe dynamics within an ice stream, but provides an inaccurate flow description outside ice streams and in

regions where there is strong basal friction balancing vertical shear stresses.

One approach to accurately describing all flow regimes within an ice sheet is to use both the above end-member models, coupling them together by imposing jump conditions at stream and shelf boundaries (Hulbe and MacAyeal, 1999; Ritz and others, 2001; Schoof, 2006). It is convenient, however, to describe the flow of an ice sheet using the same set of partial differential equations over the whole domain. Hybrid approximations provide a way of computing the leading-order flow dynamics for all flow regimes within an ice sheet without the numerical challenges of solving a full-Stokes flow system (e.g. Blatter, 1995; Bueler and Brown, 2009; Schoof and Hindmarsh, 2010; Goldberg, 2011; Winkelmann and others, 2011). In this study we derive a shallow-ice hybrid approximation, taking a similar approach to Schoof and Hindmarsh (2010) by introducing a scaling parameter related to the proportion of velocity due to slip at the bed. Other authors have taken different approaches; in particular Bueler and Brown (2009) solve the nonlinear SIA and SSA separately and then add the solutions together using an arbitrary weighting function.

Regardless of the model used for the ice flow, the accuracy of the flow description is largely due to correct computation of the basal velocity. The amount of slip that can occur at the bed is governed by the frictional resistance there, which, in turn, is intrinsically linked to bed characteristics and the subglacial hydrology (e.g. Iken and Bindschadler, 1986; Clarke, 2005). It is common to represent this response of the basal velocity to changes in basal shear stress through a sliding law (e.g. Paterson, 1994; Fowler, 2010). Since the subglacial hydrological system is complex, and relatively little is known about it due to its inaccessibility, sliding laws are typically phenomenological – they are consistent with the theory of processes governing the relationship, rather than directly derived from the physics. Single-valued sliding laws of the form $u_b = A\tau_b^n$ are long-established and still commonly used (e.g. Weertman, 1972; Fowler, 1981), but more detailed considerations of the subglacial hydrological system can suggest a variety of different relationships.

There are two contrasting types of subglacial drainage systems commonly discussed in the literature. If there is little meltwater production, the bed can be effectively drained by a distributed system of cavities, or by a simple porous flow through sediment. With increasing meltwater production, water pressure beneath the ice increases, lowering the effective pressure and hence resulting in more rapid sliding (Lliboutry, 1968; Kamb and others, 1985; Walder, 1986; Fountain and Walder, 1998). In contrast, some subglacial water transport occurs through larger-scale R othlisberger channels. These provide efficient drainage for the meltwater, resulting in low water pressure at the bed and hence lower sliding velocities (R othlisberger, 1972). Transition between these two types of drainage system can occur, for example when the discharge of meltwater has accumulated so much that a distributed system becomes over-pressurized, initializing channelized drainage (Hewitt, 2011).

The physics governing these drainage mechanisms has motivated the use of multivalued sliding laws as the basal boundary condition (Lliboutry, 1968; Hutter, 1982; McMeeking and Johnson, 1986; Fowler, 1987a,b; Kamb, 1987). Fowler and Johnson (1995, 1996) demonstrated that a ‘hydraulic runaway’ mechanism is suggestive of a triple-valued sliding law, based on the positive destabilizing

feedback between basal friction and increased meltwater production in a distributed drainage system. Sayag and Tziperman (2009) invoked a switch in drainage system as motivation for a triple-valued sliding law, suggesting that the two stable branches correspond to different drainage patterns at the bed.

However, there is more evidence for high-water-pressure, distributed drainage beneath ice sheets (Engelhardt and Kamb, 1991), and as yet no direct confirmation of the existence of R othlisberger channels beneath ice streams. Therefore, although there is evidence that before an ice stream forms the bed is already at the pressure-melting point in the onset region (e.g. Bindschadler and others, 2000), a switch in drainage systems seems an unlikely reason for ice-stream formation. In fact, the Siple Coast appears to be underlain by a layer of till (Alley and others, 1986; Blankenship and others, 1986; Tulaczyk and others, 2000b). While the driving stress on Siple Coast ice streams is 10–20 kPa (Paterson, 1994; Truffer and Echelmeyer, 2003), Engelhardt and Kamb (1991) showed through laboratory tests that the yield stress of underlying sediment is an order of magnitude smaller, and hence the till is unable to support the driving stress. The driving stress must therefore be resisted elsewhere. Physical reasoning suggests lateral shear in the ice-stream margins must provide some of this resistance, with only a small fraction balanced by friction at the bed (Echelmeyer and others, 1994; Raymond, 1996; Jackson and Kamb, 1997; Hulbe and Payne, 2001; Kamb, 2001; Truffer and others, 2001; Schoof, 2004; Sayag and Tziperman, 2008). A triple-valued sliding law has two stable branches so that the driving stress is balanced by the basal stress in both the slow- and fast-flow regimes. In contrast, a double-valued sliding law enforces a low basal stress beneath an ice stream. One therefore wonders if a double-valued sliding law also allows for ice-stream behaviour in a numerical model.

In this paper we examine the effect of the two different sliding laws on a model of ice-stream formation. We use a model that takes into account both membrane stresses and vertical shear stresses, providing a suitable description of ice flow both within and outside ice streams. Although we do not explicitly model subglacial hydrological features here, hydrological mechanisms are an important motivating factor for the relationships between basal stress and basal velocity used. The aim is to learn more about the fundamental stress balances in ice streams.

The paper is organized as follows. Section 2 provides details of the model, introducing the theory and describing the model set-up and numerical approach. In Section 3 we benchmark the model by applying a triple-valued sliding law at the bed. We extend Sayag and Tziperman’s (2009) work, investigating in more detail the triple-valued sliding law and the flow behaviour it produces. Section 4 considers behaviour under a double-valued sliding law. We find a relationship between governing parameters that allows for the formation of a stable ice stream, held back primarily by membrane stresses. In Section 5 we compare results under the two sliding laws and discuss the implications of use of the vertically integrated, higher-order formulation in comparison with the SSA.

2. MODEL DESCRIPTION

We consider an ice sheet of density ρ and viscosity η . The bedrock is at an elevation $b(x, y)$ and the surface elevation is

given by $s(x, y)$. It follows that $h = s - b$ is the thickness of the ice. The velocity in the 3-D fluid domain is given by $\mathbf{u} = (u, v, w)$. We are interested in the interior of the ice sheet where ice streams emerge. We therefore consider a patch of ice somewhere upstream of the grounding line, so that there is no need to include grounding-line or ice-shelf dynamics in the model.

2.1. Governing equations for the hybrid description of ice flow

To simplify the Stokes equation, we introduce a parameter, $\epsilon = [d]/[l]$, where $[d]$ and $[l]$ are the vertical and horizontal length scales associated with an ice sheet, with typical values provided in Table 1. Since the lateral extent of an ice sheet is much greater than its thickness (e.g. Fowler, 1997), $\epsilon = [d]/[l]$ is taken to be very small, as in lubrication theory.

For equilibrium at the ice-sheet bed, the basal drag, τ_b , resists the local driving stress, as assumed in the SIA. If, however, there is basal sliding, it is necessary to consider additional stress gradients in the model. In light of this we introduce a new dimensionless parameter, λ , which is the ratio of the magnitude of the basal stress to the viscous shear stress scale, providing an estimate of slip,

$$\lambda = \frac{[\tau_b][d]}{[\eta][u]} \leq 1.$$

When $\lambda \sim \mathcal{O}(1)$ the flow is shear-dominated (basal stresses are of similar magnitude to the vertical shear stresses) while for $\lambda \ll 1$, basal stresses are small compared with vertical shear, and the flow is sliding-dominated. λ is never >1 since $\tau_b < \eta[u]/[d]$ at all times, and equal if, and only if, the ice sheet is frozen to the bed and no slip is occurring (i.e. if the static basal stress is locally in balance with the driving stress, as in the SIA).

This parameter is similar to the traction number of Schoof and Hindmarsh (2010) and the slip ratio of Gudmundsson (2003). More specifically, if we define a deformational velocity scale due to vertical shear, $[u_d] \sim A[\tau_b]^n[d]$ (Schoof and Hindmarsh, 2010), then our parameter, λ , can be written as $\lambda = [u_d]/[u]$, which is the inverse of the slip ratio used by Gudmundsson (2003) and is closely related to the stress ratio used by Schoof and Hindmarsh (2010). An advantage of our formulation is that $0 < \lambda \leq 1$, making it easier to consider the whole range of sliding regimes, as is the purpose of using a higher-order formulation.

With ϵ and λ as the two control parameters, we derive a set of non-dimensional equations for h , u_b and v_b , as outlined in Appendix A (Fowler, 2011). We make the thin-film assumption, meaning that we neglect the horizontal gradients of the vertical shear stresses. We assume that there are no abrupt changes in basal or surface elevation, as is consistent with observations of pure ice streams. Moreover, membrane stresses are accurately approximated by using the sliding velocity to compute them; if the horizontal velocities, (u, v) , change rapidly in space, then this must be due to rapid changes in sliding velocity, (u_b, v_b) . These assumptions are explained more comprehensively in Appendix A.

The governing equation for conservation of mass is

$$\frac{\partial h}{\partial t} + \nabla \cdot \left(h\mathbf{u}_b - \lambda \frac{h^{n+2}}{n+2} |\gamma|^{n-1} \nabla s \right) = a, \tag{1}$$

where a is the accumulation rate,

$$\gamma = -\nabla s + \frac{\epsilon^2}{\lambda} \nabla \cdot \mathbf{S} \tag{2}$$

Table 1. List of notation with values of constants and scales. Typical ice-sheet scales provide a natural choice of depth and horizontal length and velocity scales. Remaining scales are chosen by balancing terms in the governing equations

Symbol	Description	Typical value
(x, y)	horizontal coordinates	
$[l]$	horizontal length scale	200 km
z	vertical coordinate	
h	depth of ice	
$[d]$	vertical length scale	1 km
s	surface elevation	
b	bed elevation	
$\partial b/\partial x$	bed slope	-5×10^{-3}
$\epsilon = [d]/[l]$	aspect ratio	5×10^{-3}
$\mathbf{u} = (u, v)$	horizontal velocity field	
$[u]$	horizontal velocity scale	500 m a^{-1}
$[t] \sim [l]/[u]$	timescale	400 years
$[\eta] \sim 1/(2[A]\tau^{n-1})$	ice effective viscosity	$6 \times 10^6 \text{ Pa}$
n	Glen's flow law exponent	1 (Newtonian) 3 (non-Newtonian)
ρ	ice density	917 kg m^{-3}
g	gravity	9.81 ms^{-2}
τ_{ij}	deviatoric stress tensor	
$\tau = \sqrt{\tau_{ij}\tau_{ij}}$	magnitude of stress	
$[\tau_b] \sim \rho g[d]\epsilon$	basal shear stress	$45\,000 \text{ Pa}$
$\lambda = [\tau_b][d]/[\eta][u]$	basal to shear stress ratio	0.015
$[a] \sim \epsilon[u]$	accumulation rate scale	2.5 m a^{-1}
$a_b(x, y)$	background accumulation	
$a_p(x, y)$	accumulation perturbation	
A_0	magnitude of a_p	

and \mathbf{S} is the resistive stress tensor (Van der Veen, 1999; Hindmarsh, 2012), given by

$$\mathbf{S} = \boldsymbol{\tau} + \mathbf{I} \text{trace}(\boldsymbol{\tau}) = \begin{bmatrix} 2\tau_{11} + \tau_{22} & \tau_{12} \\ \tau_{12} & \tau_{11} + 2\tau_{22} \end{bmatrix}. \tag{3}$$

Note that in the specific case where $\lambda > \mathcal{O}(\epsilon^2)$, γ can be approximated as

$$\gamma = -\nabla s \tag{4}$$

in Eqn (1), as is evident from an expansion of $|\gamma|^{n-1}$, retaining terms greater than $\mathcal{O}(\epsilon^2)$.

Equation (1) is a depth-integrated equation for conservation of mass. It shows that a change in depth of ice at some point is caused by divergence of the ice flux and the accumulation rate at that point. If $\lambda \rightarrow 0$ then ice flux approximates to $h\mathbf{u}_b$ (plug flow) whereas if $\lambda = 1$ the flux corresponds to that for free-surface lubrication flow (as in the SIA).

Conservation of momentum is given by

$$\begin{aligned} \tau_b &= h\gamma \\ &= -h\nabla s + \frac{\epsilon^2}{\lambda} h\nabla \cdot \mathbf{S}, \end{aligned} \tag{5}$$

which describes the force balance at the bed. The three terms correspond to basal stress, driving stress and membrane stress contributions, respectively. For $\lambda \sim \mathcal{O}(1)$, the membrane stress contribution is small and the balance is largely between the basal and driving stress; for $\lambda \ll 1$ the membrane stress correction plays a more significant role in the stress balance.

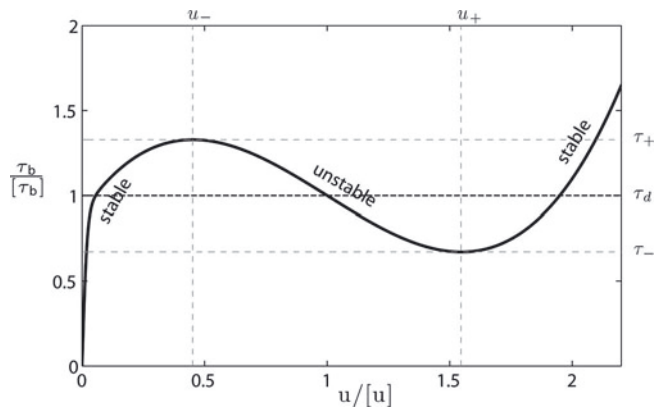


Fig. 1. A cross section of the triple-valued sliding law, $\tau_b(u, v = 0)$, based on figure 4 of Sayag and Tziperman (2009). The dashed line is the corresponding driving stress (τ_d).

2.2. Constitutive sliding law

Sliding laws of the form $\tau_b = f(\mathbf{u}_b)$ are long-established. However, because of the strong dependence of basal friction on the effective pressure at the bed, sliding laws of the form $\tau_b = f(\mathbf{u}_b, N)$, where N is the effective pressure at the bed, provide a better description. In the current framework we do not model the basal water pressure; hence we use the first kind, although some dependence on effective pressure is implicitly included in our choice of f .

More specifically, in the first part of this work we consider a triple-valued sliding law. Sayag and Tziperman (2009, 2011) developed the ideas behind such a sliding law and we adopt their implementation, which is obtained analytically from a simple one-dimensional (1-D) force balance, based on the cross-flow structure of an ice stream. Figure 1 illustrates the resulting non-dimensional relationship, given by

$$\tau_b = \frac{\mathbf{u}_b}{|\mathbf{u}_b|} \left[(|\mathbf{u}_b| - 1)^3 + \alpha(|\mathbf{u}_b| - 1) + 1 \right] \tanh(\beta |\mathbf{u}_b|), \quad (6)$$

where α and β are parameters taken to be -0.9 and 50 , respectively.

A multivalued sliding law is expected to be unstable on its middle branch where $\partial\tau_b/\partial u_b < 0$ (Lliboutry, 1968, p.55). Consequently, if the stress is gradually increased while on the lower branch to the first maximum in Figure 1, a transition must then occur to the upper branch, and this transient must involve the rapid variation of some other dynamical quantity that is implicitly involved in the sliding law. Commonly, this hidden variable is taken to be the subglacial effective pressure, which is also presumed to be the underlying cause of the multivaluedness (Fowler, 1987b). We therefore introduce a new variable, ν , such that

$$\delta \frac{\partial \nu}{\partial t} = |\mathbf{u}_b| - \nu, \quad (7)$$

where δ is a parameter that describes the timescale on which ν relaxes to \mathbf{u}_b , i.e. a timescale for the evolution of the subglacial drainage system. This timescale introduces a limit to how rapidly velocities can transition between u_- and u_+ .

By replacing \mathbf{u}_b with ν in the part of the triple-valued sliding law that governs the positioning of the unstable branch (the cubic polynomial), we obtain a relationship between basal stress and velocity with some time dependence in it, defining a timescale over which velocity changes

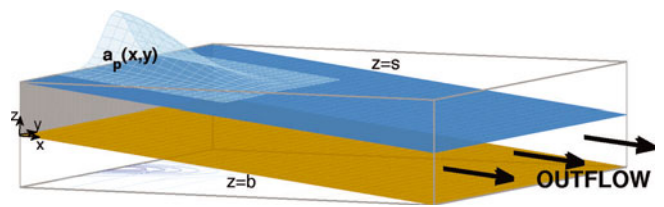


Fig. 2. Schematic illustrating the model set-up. The bed is flat and of constant slope. The surface is also flat initially, before a constant perturbation to the accumulation field is applied in the form of a Gaussian blob, $a_p(x, y)$, as illustrated. There is zero inflow at the $x = 0$ boundary.

in response to changes in basal stress. In particular, taking $\delta = 10^{-3}$ gives a timescale of evolution for the system of 0.4 years, given the other scales in Table 1.

The triple-valued sliding law hence becomes

$$\tau_b = \frac{\mathbf{u}_b}{|\mathbf{u}_b|} \left[(\nu - 1)^3 - \frac{9(\nu - 1)}{10} + 1 \right] \tanh(50|\mathbf{u}_b|). \quad (8)$$

We propose that sliding laws of the form $\tau_b = f(\mathbf{u}_b)$ which express a physically unstable relationship between τ_b and u_b should be replaced with those of the form $\tau_b = f(\mathbf{u}_b, \nu)$.

2.3. Model set-up and numerical solution

Figure 2 shows the 3-D model set-up. There is zero inflow into the domain at $x = 0$, implemented by setting $u_b = 0$ and $\partial s/\partial x = 0$; the latter imposes zero flow due to vertical shear at $x = 0$. Free slip is allowed along the boundary ($\tau_{12} = 0$). To avoid considering grounding-line behaviour, we treat $x = 1$ as an open outflow boundary (Papanastasiou and others, 1992; Sayag and Tziperman, 2009), where the upper surface is free to evolve and $\partial u/\partial x = 0$. The domain is periodic in the y -direction.

The simulations are initialized in a steady state that is uniform in the cross-flow direction. Downstream of the inflow boundary the ice has a constant thickness, $h = 1$. There is no variation in velocity in the cross-flow direction, i.e. $(u, v) = (u(x), 0)$. Under these conditions, the velocity field can be computed from Eqns (5) and (8), with $\nu = |\mathbf{u}_b|$ in the steady state. A background ‘balance’ accumulation, $a_b(x)$, is required to maintain the steady state. This balance accumulation is the steady-state solution of Eqn (1), given by

$$a_b(x, y) = \frac{\partial u_b}{\partial x}. \quad (9)$$

A forcing is required to produce ice-stream behaviour. A perturbation accumulation, $a_p(x, y)$, is therefore also applied, in the form of a truncated Gaussian at the upper boundary (motivated by Sayag and Tziperman, 2009). More specifically, $a_p(x, y)$ is given by

$$a_p(x, y) = A_0 \exp \left[-25x^2 - 100 \left(y - \frac{1}{2} \right)^2 \right], \quad (10)$$

where A_0 is the magnitude of the perturbation. The magnitudes used are necessarily large, but can be thought of as representing the sum of accumulation rates from upstream. Use of such a forcing provides a simple way of reproducing ice-stream behaviour, which allows us to study the resulting downstream flow regimes.

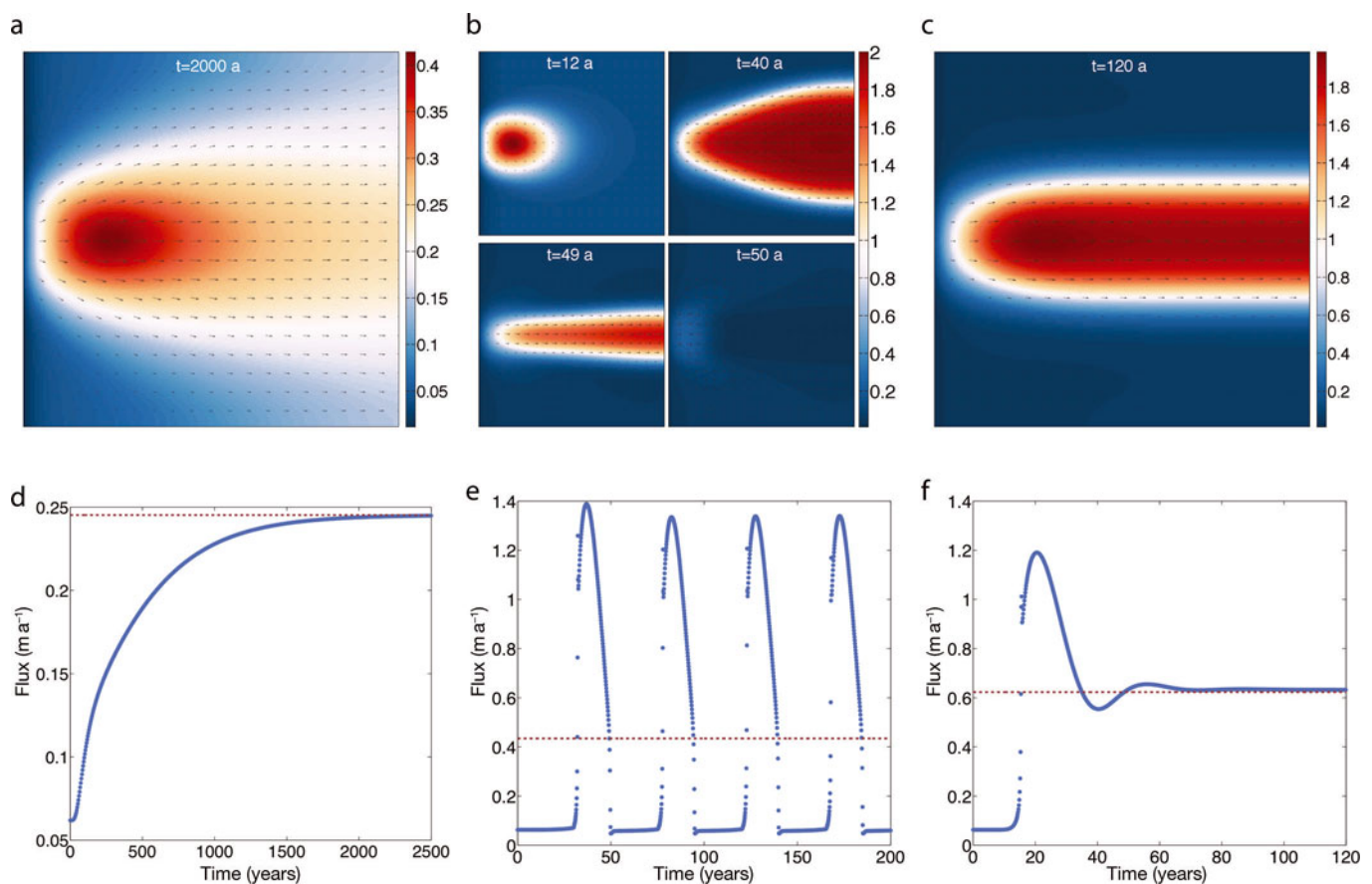


Fig. 3. Simulation results for three different incoming mass flux values ($A_0 = 15 \text{ m a}^{-1}$, 30 m a^{-1} and 45 m a^{-1} for (a, d), (b, e) and (c, f), respectively). The plots in the top row are illustrations of the non-dimensional velocity fields, and the plots on the bottom row show time series of the total flux out of the solution domain (blue dots plotted at regular time intervals), with the total incoming flux also plotted (red dashed line).

We discretize the governing equations and boundary conditions using a finite-difference scheme with semi-implicit time-stepping. We use a staggered, Cartesian, two-dimensional (2-D) grid with $n_i \times n_j$ discrete points (Rommelaere and Ritz, 1996; Sayag and Tziperman, 2009). An upwind difference scheme is implemented at the open outflow boundary, together with the condition $\partial u / \partial x = 0$ (Sayag and Tziperman, 2009). The nonlinear system of equations is solved using a Newton–Krylov solver, provided by the Portable Extensible Toolkit for Scientific Computation (Balay and others, 1997, 2012a,b). The fully coupled system is inverted at each time-step, and the solution is accepted when the absolute size of the nonlinear system residual is $< 10^{-8}$. To aid numerical solution, if this condition is not satisfied after 50 iterations we split the equations into two groups (Eqns (1) and (7) in one, and the components of Eqn (5) in the other) and solve them iteratively using a Picard iteration with a subspace correction (Hindmarsh and Payne, 1996). The code is tested against two analytic solutions, as outlined in Appendix B. The code converges to the steady-state solutions rapidly and the accuracy of the agreement is good.

Values of constants are given in Table 1. The value of the maximum time-step must always be smaller than the relaxation timescale defined by δ so that changes in velocity are not limited by the size of the time-step.

An alternative set-up, together with some basic results, is discussed in Appendix C.

3. RESULTS WITH A TRIPLE-VALUED SLIDING LAW

3.1. Reference flow regimes at small λ

In order to assess the suitability of the model for describing ice dynamics in and outside ice streams, we apply the triple-valued sliding law as the basal boundary condition in the set-up described in Section 2.3. The ice rheology is taken to be Newtonian, to allow us to compare results with Sayag and Tziperman (2009).

Figure 3 shows the three distinct flow regimes that occur as a result of varying the magnitude of the perturbation accumulation, A_0 . Other parameter values are given in Table 1.

In Figure 3a, for a small value of A_0 , the solution reaches a steady state in which the velocities all fall on the slow, stable branch of the sliding law and the influx is dispersed across the domain. Figure 3d shows the evolution of the total flux out of the domain, which reaches a steady state after ~ 2000 years.

In Figure 3b, for a slightly larger value of A_0 , solutions oscillate between slow-flow and fast-flow behaviour. Initially the velocity field falls entirely on the slow branch of the sliding law. As the accumulation builds up near the inflow boundary, increasing the surface slope, the velocity moves to the fast stable branch of the sliding law and an ice stream forms downstream of the perturbation. The ice stream evolves, drawing down the additional upstream mass accumulation, until there is no longer a driving stress

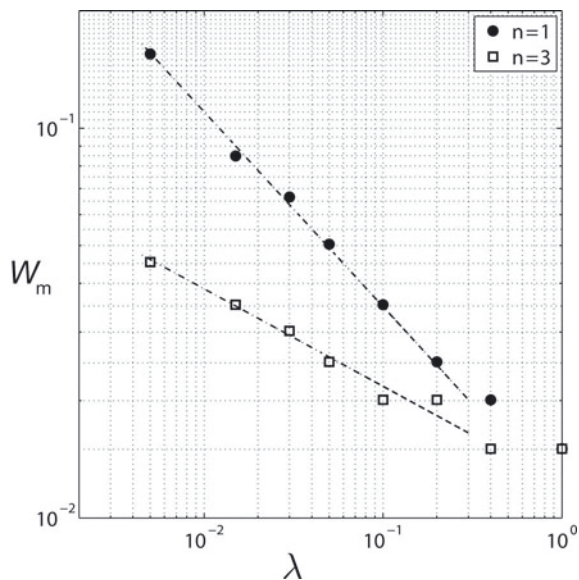


Fig. 4. A plot showing how the shear margin width of an ice stream varies with the scaling parameter, λ . Results from simulations run with $n = 1$ and 3 are both plotted, where n is Glen's flow law exponent. Dashed lines with gradient $-1/(n + 1)$ are also plotted.

sufficient to maintain the stream. The ice stream narrows before collapsing back to its no-stream state. The cycle then repeats.

Finally, in Figure 3c, further increasing the magnitude of the perturbation accumulation, A_0 , results in sustained flow on the fast, stable branch of the sliding law. A steady-state stream forms, with different regions of the domain on different branches of the sliding law.

These are the same three distinct flow regimes that were reported by Sayag and Tziperman (2009), who used the same set-up, but solved the SSA. The regimes illustrated in figures 5–7 in their work directly correspond to those shown in Figure 3 here. We have neglected to include the depth fields and cross-stream velocity profiles, as the most interesting behaviour is captured in the plots included here. Quantitative differences occur between our results and theirs for a given accumulation perturbation, due to the use of a higher-order formulation in our work, which accounts for vertical variation in horizontal velocities. Particularly in regions of low basal velocity, the added component of velocity at the ice surface due to vertical shear is significant, and results in larger outflow from the domain for a given basal velocity. A further difference arises from the addition of the parameter ν into the sliding law (Eqn (8)). It makes our solver convergence more rapid and more robust. Moreover, the jumps in velocity in the solutions are less rapid and the overall behaviour is smoother, as can be seen by direct comparison of Figure 3e and f with figures 7a and 6a, respectively, in Sayag and Tziperman (2009). Setting $\delta = 0$ (i.e. taking $\nu = |\mathbf{u}_b|$), results in behaviour as seen by Sayag and Tziperman (2009), with rapid jumps in flux when the solution moves across the unstable branch of the sliding law (e.g. in the region 11–12 years in figure 6a of their paper).

3.2. Variations in λ

Having verified (Section 3.1) that our formulation reproduces the three flow regimes obtained by Sayag and Tziperman (2009), we diverge from their study to look at

the effect of including vertical variation in horizontal velocity due to gravity-driven shear. We do so by varying the scaling parameter, λ , corresponding to the basal-to-shear-stress ratio, and looking at the impact on emergent ice-stream behaviour. A value of $\lambda \ll 1$ corresponds to attributing most of the movement to sliding when considering the stress balance (as in the SSA), while $\lambda = 1$ corresponds to assuming that all velocity is due to vertical shear (as in the SIA). Intermediate values correspond to various different proportions of the velocity being attributed to sliding when considering the stress balance.

3.2.1. Shear margin width

The value of λ affects the characteristics of an ice stream that forms under this formulation. We consider a simple model of an ice stream where the cross-stream velocity component, v , is zero, and u only varies in the cross-stream direction (Sayag and Tziperman, 2011). Figure 3c shows this to be a fair description for a steady-state ice stream downstream of the onset zone.

Under these simplifications, the only non-trivial, non-dimensional governing equation is

$$\tau_{13}(b) = -h \frac{\partial s}{\partial x} + \frac{\varepsilon^2}{\lambda} h \frac{\partial}{\partial y} \left(\frac{1}{\tau^{n-1}} \frac{\partial u_b}{\partial y} \right), \quad (11)$$

where

$$\tau^2 = \tau_{13}^2 + \frac{\varepsilon^2}{\lambda^2} \tau_{12}^2. \quad (12)$$

Assuming that vertical shear is negligible compared with lateral shear in the stream itself, we have $\tau_{13} \ll (\varepsilon/\lambda)\tau_{12}$. This assumption means τ^2 can be approximated as $(\varepsilon^2/\lambda^2)\tau_{12}^2$, giving

$$\tau^{n-1} = \left| \frac{\varepsilon}{\lambda} \frac{\partial u_b}{\partial y} \right|^{1-\frac{1}{n}}. \quad (13)$$

We now seek the distance, W_m , corresponding to the velocity drop, ΔU , across the shear margin. Assuming a balance between the driving stress and horizontal shear in the margins, we obtain the relation

$$(W_m)^{1+\frac{1}{n}} \sim \frac{\varepsilon^{1+\frac{1}{n}}}{\lambda^{\frac{1}{n}}} (\Delta U)^{\frac{1}{n}}. \quad (14)$$

Now the value of ΔU is enforced by the triple-valued sliding law (and corresponds to $(u_+ - u_-)$ in Fig. 1). The shear margin must therefore obey

$$W_m(n, \lambda) = \varepsilon K_1^{\frac{n}{n+1}} \left(\frac{K_2}{\lambda} \right)^{\frac{1}{n+1}} \quad (15)$$

for constants K_1 and K_2 .

Taking logarithms of Eqn (15) gives

$$\log(W_m) = \log(\varepsilon) + \frac{n}{n+1} \log(K_1) + \frac{1}{n+1} \log(K_2) - \frac{1}{n+1} \log(\lambda), \quad (16)$$

suggesting that a logarithmic plot of W_m against λ should give a straight line with gradient $-1/(n + 1)$.

Figure 4 is a plot of margin width against λ from results of simulations run on a 200×200 grid. The circles correspond to Newtonian viscosity ($n = 1$) and the squares to non-Newtonian viscosity ($n = 3$). Lines with gradients $-1/2$ and $-1/4$ are plotted through the Newtonian and non-Newtonian points, respectively. The horizontal gridlines are plotted at intervals of the grid spacing in the simulations.

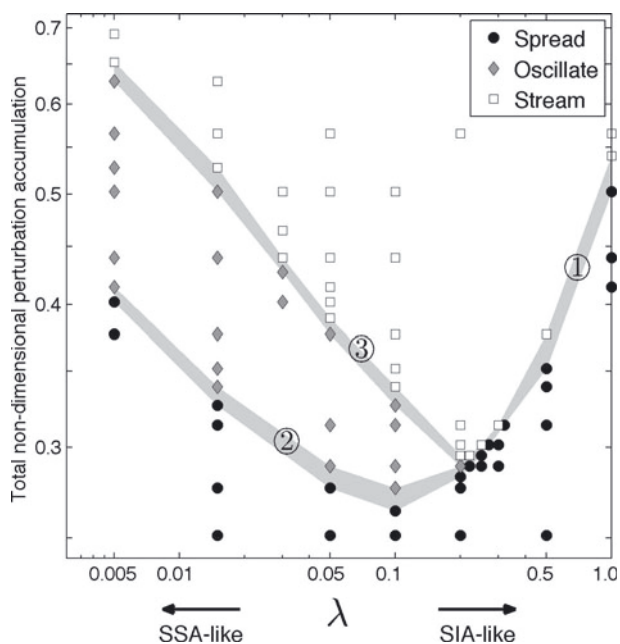


Fig. 5. Phase diagram showing three discrete regions for slow, fast and oscillatory behaviour. Each point plotted represents one simulation that was run with specified values of λ and A_0 .

The margin width decreases as λ increases, since membrane stresses play a less dominant role in the stress balance. Without membrane stresses, large jumps in velocity are allowed to occur over a small distance. Moreover, when the margin width is small and spans only two or three gridpoints, it can only take one of a few discrete values, given the choice of resolution. We therefore see that the lines with gradient $-1/(n + 1)$ in Figure 4 are a very good fit to the plotted points, only losing accuracy for numerically unresolved margin widths.

3.2.2. Effect of λ on flow regime

We also address the question of how the choice of λ affects flow behaviour across all flow regimes with an ensemble of simulations. Values of λ and A_0 are different in each simulation. Figure 5 maps the resulting flow regimes for different parameter combinations. All three distinct flow regimes occur, each plotted with a different marker; the divides between flow regimes in parameter space are shaded and labelled numerically. We discuss each of these boundaries and explain the physical processes that govern where the boundaries lie in parameter space.

Boundaries 1 and 2 separate solutions that remain at all times on the slow stable branch of the sliding law (dark circles in Fig. 5) from those that exhibit some oscillatory or streaming behaviour (grey diamonds and white squares in Fig. 5, respectively). The minimum perturbation to the accumulation field large enough to cause the flow to move onto the fast branch of the sliding law occurs at $\lambda \approx 0.1$. For $\lambda < 0.1$ the required size of the perturbation accumulation increases as λ decreases further (divide 2), and similarly, for $\lambda > 0.1$, the size of a_p must be increased further for there to be any solutions that exhibit fast-flow behaviour (divide 1).

In a bid to explain these observations we consider the necessary conditions for the flow to enter the fast-flow regime. As a result of implementing the triple-valued sliding law, the basal stress must reach a critical value, τ_+ (Fig. 1)

before transitioning onto the unstable branch of the sliding law. Equation (5) describes a balance between basal stress and driving stress, with a correction of $\mathcal{O}(\varepsilon^2/\lambda)$ due to membrane stresses. For expository simplicity, we write it as

$$\begin{aligned} \text{(basal stress)} &= \text{(driving stress)} \\ &+ \frac{\varepsilon^2}{\lambda} \text{(depth-integrated membrane stress gradients)}. \end{aligned} \tag{17}$$

When $\lambda \sim 1$ the correction for membrane stress effects is $\mathcal{O}(\varepsilon^2)$, and so to $\mathcal{O}(\varepsilon^2)$ accuracy the balance is between driving and basal stress, as in the SIA. When the driving stress in the onset region reaches the critical value, τ_+ , the transition onto the unstable branch of the sliding law occurs and there is resulting fast-flow behaviour. The correction for membrane stresses, however, becomes more significant for smaller values of λ and so influences how large the driving stress, $-h\partial s/\partial x$, needs to become before the basal stress reaches the critical value. In turn, the rate at which the accumulation builds up in the onset zone controls this increase in driving stress. The build-up further depends on the rate at which the incoming ice is drawn downstream. We hence consider the non-dimensional flux out of the domain, which in the Newtonian case, with bed-slope gradient -1 and constant depth field 1 (as is the case for ice streams which form in this suite of simulations), is given by

$$\begin{aligned} q_x &= \int_0^1 \left[u_b(1, y) + \frac{\lambda}{3} \right] dy \\ &\approx U_s W_s + \frac{\lambda}{3}, \end{aligned} \tag{18}$$

where U_s is the transversely averaged stream velocity and W_s the width of the ice stream. It is evident that, when $\lambda \sim \mathcal{O}(1)$, the increased flux due to vertical shear can be significant, whereas when λ is small this effect is insignificant.

For boundary 1 in Figure 5, $\lambda \gtrsim 10^{-1}$, and hence the membrane stress correction in Eqn (17) is negligible. Equation (18) shows that as λ increases there will be a resultant increase in outflow from the domain for a given basal velocity. For a given basal velocity field, more ice is therefore removed with higher values of λ ; hence less ice accumulates in the onset region where the accumulation perturbation is applied. A larger a_p is required at higher λ for the driving stress to reach the critical value to cause transition onto the unstable branch of the sliding law (τ_+ in Fig. 1). This explains the positive gradient of curve 1 for $\lambda \gtrsim 10^{-1}$.

The curve defining boundary 2 in Figure 5, in contrast, has a negative gradient. For smaller values of λ , the flow velocities remain completely on the slow branch of the sliding law for much larger accumulation rates. At these lower values of λ , $\lambda/3$ is small and so the outflow (Eqn (18)) depends only on u_b . It is necessary then to consider the effect of the membrane stress correction in the stress balance (Eqn (17)). While for $\lambda \gtrsim 10^{-1}$ the dominant balance is between the basal stress and the driving stress, as λ decreases further, the $\mathcal{O}(\varepsilon^2/\lambda)$ correction in Eqn (17) becomes more significant. The greater accumulation in the onset region causes the driving stress to increase. The increasing velocity in the onset region results in large negative gradients in the longitudinal stress, since the velocities downstream are lower. The $\mathcal{O}(\varepsilon^2/\lambda)$ correction is therefore negative, meaning that the driving stress needs to reach larger values before the right-hand side of Eqn (17) will reach the critical value, τ_+ , at

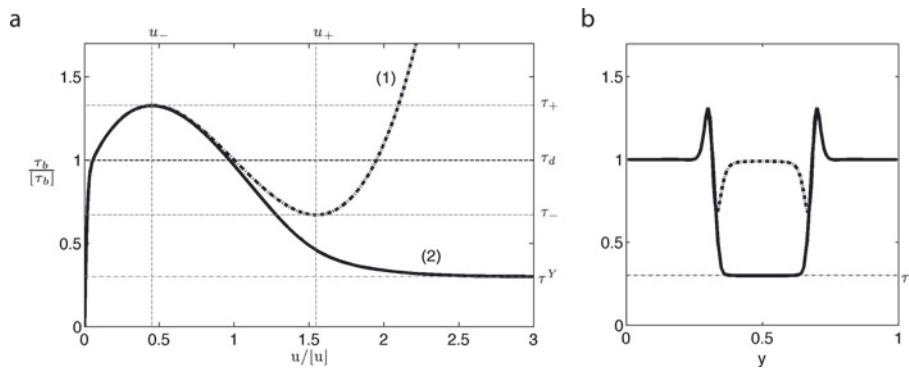


Fig. 6. Comparisons between the triple-valued and double-valued sliding laws. (a) Cross-sections of the triple-valued sliding law (dashed curve) and double-valued sliding law (solid curve). (b) Schematic of the cross-stream basal stress profiles, $\tau_b(u, v = 0)$. They are taken across an ice stream formed with the triple-valued sliding law (dashed curve) and the double-valued sliding law (solid curve) as the basal boundary conditions.

which the transition to the unstable branch of the sliding law will occur. This effect is only further amplified as λ decreases further, and so larger perturbations to the accumulation field are required to reach the higher driving stresses that result in oscillatory/streaming behaviour. This explains the negative gradient of the curve separating the slow flow behaviour and oscillatory/streaming behaviour for $\lambda \lesssim 10^{-1}$. Since lower values of λ correspond to a stress balance where membrane stresses are of increased significance, this result emphasizes the important effect membrane stresses can have in inhibiting the emergence of ice streams.

Finally we consider what governs boundary 3, which separates flow that periodically surges from those solutions that form a steady-state stream. There is no oscillatory flow once this boundary intersects boundary 1, for $\lambda \gtrsim 0.2$. For a steady-state stream to exist, the outflow from the domain must balance the incoming mass accumulation perturbation, $\int \int a_p(x, y) dx dy$. Equation (10) gives an expression for a_p that can be integrated:

$$\int \int a_p(x, y) dx dy = \int_0^1 \int_0^1 A_0 e^{-25x^2 - 100(y-\frac{1}{2})^2} dx dy \approx \frac{\pi A_0}{100}, \tag{19}$$

giving the total incoming perturbation accumulation.

Equating the outflow (Eqn (18)) and the incoming mass accumulation (Eqn (19)) gives

$$\frac{\pi A_0}{100} = U_s W_s + \frac{\lambda}{3}. \tag{20}$$

Equation (20) gives the necessary condition that must be satisfied for a solution to form an ice stream. If there is enough incoming mass accumulation to maintain a stream of width W_s , the solution will form a steady-state stream; if there is not, the solution will oscillate. Given that the flux in a stream is given by Eqn (18), why then does a solution with a smaller value of λ need more accumulation before a steady-state stream can form? It is due to the fact that a smaller value of λ results in stresses being delocalized and so results in wider shear margins, as discussed in Section 3.2.1. We therefore have a wider strip of the domain flowing at higher velocities and hence greater outflow from the domain at smaller λ . Consequently more incoming mass accumulation is required with smaller values of λ to be able to maintain the resulting wider streams.

4. RESULTS WITH A DOUBLE-VALUED SLIDING LAW

While there are physical mechanisms involving meltwater drainage feedbacks that motivate the choice of a triple-valued sliding law (Fowler and Johnson, 1995; Sayag and Tziperman, 2009), some of these effects are more common on a seasonal timescale and hence probably more relevant as controlling mechanisms for seasonal surges (e.g. Schoof, 2010). In Antarctica, studies suggest the till behaves more like a plastic material with a yield stress (Alley and others, 1986; Blankenship and others, 1986). The triple-valued sliding law does not represent such behaviour well; Figure 6 illustrates that under the triple-valued law, the modelled basal stress beneath an ice stream is as high as that outside the stream.

McMeeking and Johnson (1986) suggested a sliding law, such as curve (2) in Figure 6a, to be a good way of representing physical processes occurring at the bed. The existence of a critical velocity, u_- , at which the base fails was one possible explanation they provided, along with the possibility of the high stresses at a surge front disrupting the in situ drainage system, perhaps closing off a channelized system.

We ran some simple experiments with a doubled-valued sliding law as our basal boundary condition to investigate the stress balances in ice streams that slide over a base capable of supporting only low stresses ($\leq \tau^Y$, where τ^Y is yield stress of the basal sediment) at high velocities. One might think that the ice stream could now run away due to the low basal resistance at the bed, but in practice this does not happen; the driving stress is, instead, resisted by lateral shear stresses in the ice-stream margins.

For ease of comparison, and to enable the use of the same model set-up, we formulate a sliding law using tanh functions to reshape the function given by Eqn (8). Given that our triple-valued law can be written as $\tau_b = \frac{\mathbf{u}_b}{|\mathbf{u}_b|} f(\nu, |\mathbf{u}_b|)$, we have

$$\tau_b = \frac{\mathbf{u}_b}{|\mathbf{u}_b|} \left\{ \frac{1}{2} f(\nu, |\mathbf{u}_b|) [1 - \tanh(3\nu - 4.5)] + \frac{1}{2} \tau^Y [1 + \tanh(3\nu - 4.5)] \right\}, \tag{21}$$

where ν is as defined in Eqn (7). Figure 6a is a plot of this function alongside the original triple-valued function (dashed curve).

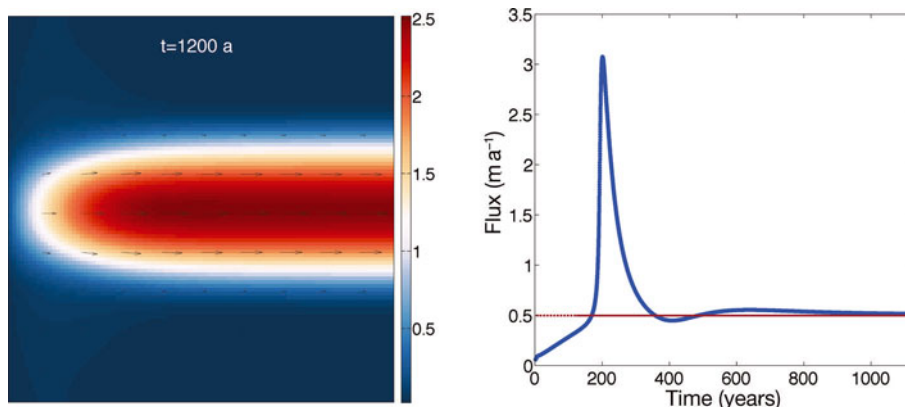


Fig. 7. An example simulation for which a steady-state stream forms with $n = 1$, $\lambda = 0.005$, $\tau^Y = 0.3$, $A_0 = 35 \text{ ma}^{-1}$, $\delta = 0.1$ and all other parameter values given in Table 1.

4.1. Steady-state ice streams under a double-valued sliding law

To see the effect of using a double-valued sliding law on ice-stream formation, we ran a set of simulations similar to those in Section 3. For small accumulation perturbations these exhibit the same behaviour as with a triple-valued sliding law (as expected, due to the sliding laws overlying each other at low velocities). It is the behaviour on the unstable branch that is of interest; under what parameter combinations can a stable stream-like solution be maintained?

Experimentation shows that under most parameter combinations, a solution to the governing equations resulting in a steady-state stream is not possible. Streams that form increase in velocity rapidly (there are insufficient stresses to hold them back) and since there is limited incoming accumulation a balance is not possible, i.e. Eqn (20) cannot be satisfied, and so the code stops converging unless membrane stresses increase quickly enough to hold back the stream. As such, only under very specific combinations of parameters does a fully coupled nonlinear evolution of the governing equations with the double-valued sliding law (Eqn (21)) reach a steady-state stream solution. Figure 7 gives an example of one solution resulting in a steady-state Newtonian stream.

Note that there are a number of parameters in the sliding law neither constrained by observations nor directly related to the physics (e.g. the smoothing parameter, δ , the value of τ_+ at the peak of the sliding law and the magnitude of the accumulation perturbation). The large parameter space means it is difficult to choose the most representative values of all the parameters.

4.2. A simpler model for an ice stream underlain by weak till

To determine the parameter combination needed for a steady-state stream to form under the double-valued sliding law, we consider a simple model of an ice stream and ascertain the balance of terms when the basal stress is not providing full resistance to the stream. The cross-stream velocity component is taken to be zero ($v = 0$) and u is taken to vary only in the cross-stream direction (i.e. u is a function of y only, as for the shear-margin-width scaling in Section 3.2.1). The domain is taken to be of constant depth, $h = 1$, and so $\nabla s = \nabla b = (-\alpha, 0)$. (We use $\alpha = 1$ for the simulations run in this paper, but we carry out this scaling analysis for the most general case.)

Under these simplifications the only non-trivial governing equation is

$$\tau_{13}(b) = \alpha + \frac{\epsilon^2}{\lambda} \frac{\partial}{\partial y} \left(\frac{1}{\tau^{n-1}} \frac{\partial u_b}{\partial y} \right), \tag{22}$$

where

$$\tau^2 = \tau_{13}^2 + \frac{\epsilon^2}{\lambda^2} \tau_{12}^2. \tag{23}$$

As for the shear-margin-width scaling, vertical shear within the stream is taken to be negligible compared with lateral shear across the margins, meaning that τ^2 can be approximated as $(\epsilon^2/\lambda^2)\tau_{12}^2$ and

$$\tau^{n-1} \approx \left| \frac{\epsilon}{\lambda} \frac{\partial u_b}{\partial y} \right|^{1-\frac{1}{n}}. \tag{24}$$

We also assume a yield stress of the basal sediment beneath the ice stream, τ^Y . Hence $\tau_{13}(b) = \tau^Y$ in Eqn (22) and it becomes

$$\tau^Y \approx \alpha + \frac{\epsilon^{\frac{1}{n}+1}}{\lambda^{\frac{1}{n}}} \frac{\partial}{\partial y} \left(\left| \frac{\partial u_b}{\partial y} \right|^{\frac{1}{n}-1} \frac{\partial u_b}{\partial y} \right). \tag{25}$$

Integrating Eqn (25) in y and applying the centre-line condition, $\partial u_b / \partial y = 0$ at $y = 0$, we get

$$\left| \frac{\partial u_b}{\partial y} \right|^{\frac{1}{n}-1} \frac{\partial u_b}{\partial y} = \left(\frac{\lambda}{\epsilon} \right)^{\frac{1}{n}} \frac{1}{\epsilon} (\tau^Y - \alpha) y. \tag{26}$$

Assuming the highest velocity is at the centre of the ice stream, this simplifies to

$$\frac{\partial u_b}{\partial y} = -\frac{\lambda}{\epsilon^{n+1}} |\tau^Y - \alpha|^n |y|^{n-1} y \tag{27}$$

and we now have

$$u_b = u_b(0) - \frac{\lambda}{\epsilon^{n+1}} \frac{|\tau^Y - \alpha|^n |y|^{n+1}}{n+1}. \tag{28}$$

This describes a velocity profile across an ice stream under our model formulation with a double-valued sliding law.

Furthermore, defining W_s to be the width of an ice stream, $u_b(\pm W_s/2) = u_\infty$ to be the basal velocity outside that ice stream (usually close to zero), and taking $\Delta U = u(0) - u_\infty$, results in

$$\Delta U = \frac{\lambda}{\epsilon^{n+1}} \frac{|\tau^Y - \alpha|^n}{n+1} \left(\frac{W_s}{2} \right)^{n+1}, \tag{29}$$

as a relationship between the non-dimensional velocity

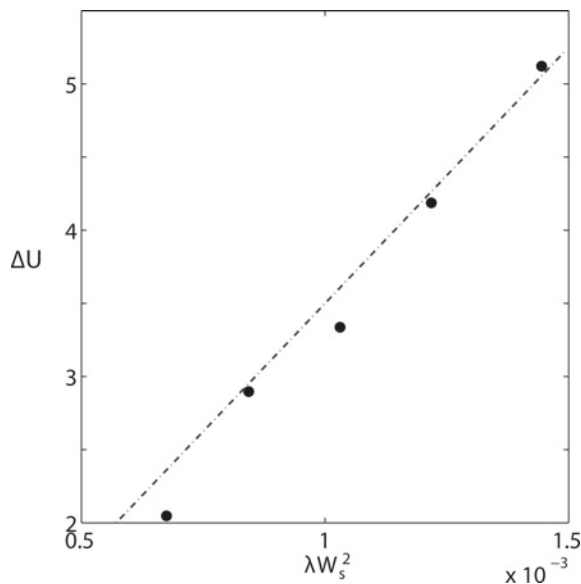


Fig. 8. Plot of ΔU against λW_s^2 , showing the fit of our results to the scaling ($\Delta U = 3500\lambda W_s^2$ is the line plotted).

change between the inside and outside of the stream and the non-dimensional width of the ice stream, the basal yield stress of the underlying till, the bed slope and the controlling parameters, λ and ε . This is the well-known result for a parabolic velocity cross-profile of an ice stream (e.g. Raymond, 1996; Van der Veen, 1999), but also includes the dependence on the controlling model parameters, ε and λ .

For example, given ice with non-Newtonian rheology ($n = 3$), and taking our typical scalings for an ice sheet, $\varepsilon = 0.005$ and $\lambda = 0.015$ (Table 1), we have

$$\Delta U = (3.75 \times 10^5) |\tau^Y - \alpha|^3 W_s^4. \quad (30)$$

Typical driving stresses for pure ice streams are in the region of 10–20 kPa (Raymond, 1996; Truffer and Echelmeyer, 2003) with basal stresses of ~1–10 kPa (Sayag and Tziperman, 2009). Taking $|\tau^Y - \alpha| \sim 10^{-1}$, we get the result that ice streams with velocities in the range 10^2 – 10^3 m a^{-1} , as in the Siple Coast, will be between ~30 and 60 km wide, which is in agreement with observations (e.g. Paterson, 1994).

Furthermore, in Section 4 we experimented with simulations using Newtonian rheology ($n = 1$), $\alpha = 1$, $\tau^Y = 0.3$ and varying values of λ and accumulation magnitude. Equation (29) suggests they therefore should obey

$$\Delta U = 3500\lambda W_s^2; \quad (31)$$

and we illustrate this behaviour with a plot of ΔU against λW_s^2 in Figure 8. The deviation from the scaling is due to numerical inaccuracies, as the width of the ice stream is very sensitive to numerical resolution. The simulations for Figure 8 were run with $n_i = n_j = 100$.

It is important to note that the simulations run to create this figure do not all necessarily lie within physical parameter space: the velocities span a much wider range than that found in nature. Moreover, this scaling explains why there is such sensitivity to changes in parameters. Given a certain basal stress underneath the stream, the membrane stresses are only sufficient to hold back the stream if the combination of parameters chosen satisfies Eqn (29).

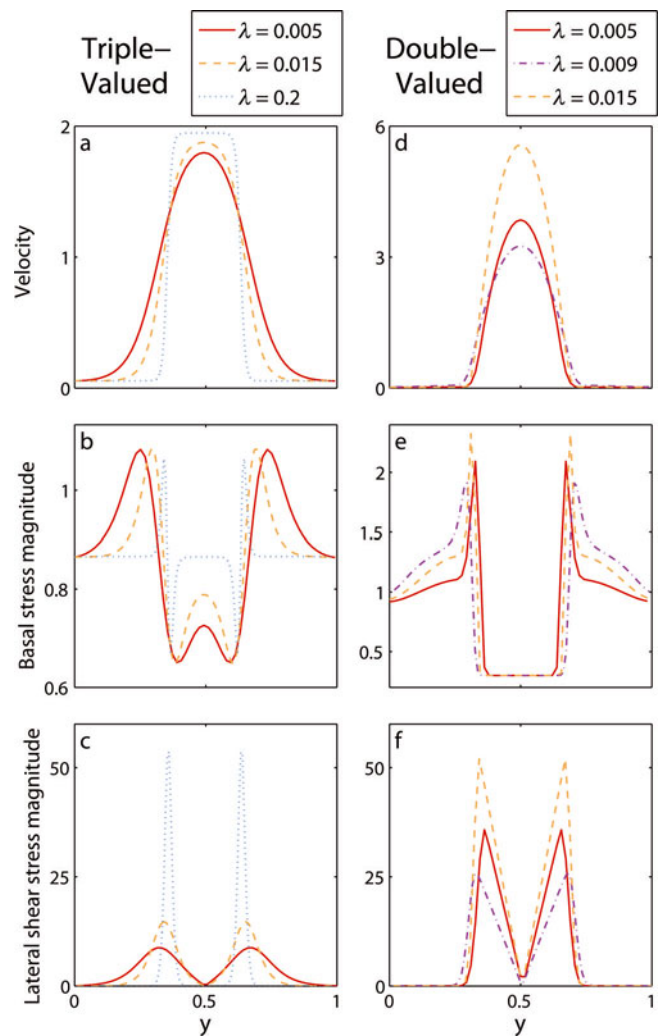


Fig. 9. Cross-stream velocity and stress profiles for ice streams formed under a triple-valued sliding law (left column) and a double-valued sliding law (right column). (a) and (d) show the cross-stream velocity profiles. (b) and (e) show the corresponding profiles of basal stress magnitude, $\sqrt{|\tau_{13}|^2 + |\tau_{23}|^2}$, and (c) and (f) the corresponding lateral shear stress magnitude, $|\tau_{12}|$.

5. DISCUSSION

5.1. Comparison of stress fields under the two sliding laws

We now consider in detail the stress balances in ice streams that occur as a result of contrasting sliding laws. Figure 9 shows cross-stream velocity profiles for streams formed under both triple-valued and double-valued sliding laws, and the corresponding plots of the magnitude of basal stress and lateral shear stress.

Figure 9a illustrates how the cross-stream velocity profile changes with variation in λ under the triple-valued sliding law. Narrowing of the shear margins at higher values of λ , as discussed in Section 3.2.1, can be seen clearly.

Figure 9b shows how the corresponding distribution of the basal stress changes with variations in λ . As λ decreases, increasing the significance of the membrane stresses in the stress balance, the delocalizing effect of the membrane stresses means the basal stresses do not increase back to the stable value within the width of the ice stream. Only at higher values of λ , when the margins are narrower, do the

basal stresses rapidly increase to be in balance with the driving stress. The behaviour of the basal stress within the shear margin itself is complex. The stress field at first increases while moving from the slow-flow region into the stream, corresponding to an increase in τ_b from the intersection point of the stable branch of the triple-valued sliding law with the line $\tau_b = \tau_d$ to the value of τ_+ at the peak of the sliding law. It then decreases rapidly as the velocity increases to the inner ice-stream velocity, consistent with a decrease in basal stress along the unstable branch of the sliding law. This provides a physically plausible profile, if we assume that outside the ice stream the bed is frozen, and across the shear margin there is a transition to temperate bed conditions, due to the increased internal and frictional heating as velocities rapidly increase (Schoof, 2012). The fast-flowing ice in the stream results in large horizontal shear across the margin (Fig. 9c), and the basal friction increases due to the increasing velocity. These two effects will cause increased heating, both internally and at the bed, and so further into the margin the temperature will reach the melting point, resulting in internal and basal melting. The meltwater will lubricate the bed, causing a rapid decrease in basal friction while moving further into the ice stream, and reaching a minimum inside the shear margin.

Finally, Figure 9c shows the corresponding distribution of lateral shear stress through an ice stream with a triple-valued sliding law as the basal boundary condition. There are maxima in the lateral shear in the margins, where the rapid transition from slow flow to streaming flow occurs. At high λ these peaks in longitudinal shear stress magnitude are restricted to narrower bands. As a consequence, the lateral shear stress is of larger magnitude in these bands because the same velocity change occurs over a smaller distance ($\partial u_b / \partial y$ is larger).

Figure 9d–f correspond to Figure 9a–c, but are results with a double-valued sliding law. The velocity in the ice stream is no longer defined by the sliding law, but instead by the scaling, Eqn (29). The velocity of a steady-state stream increases linearly with λ , given a specified ice-stream width. The choice of λ is therefore critical in governing whether a stable stream can form in the model or not, once the magnitude of the forcing accumulation perturbation has been chosen (which, in turn, governs what width and velocity of ice stream can form, according to Eqn (20)).

Figure 9e shows the basal stress profiles across ice streams formed with the double-valued sliding law. At higher values of λ the peak of the sliding law (given by the value $\tau_b = \tau_+$ in Fig. 6a) is increased and hence there are larger values of basal stress in the margins when compared with the triple-valued sliding law. If the maximum was only as large as for smaller values of λ , the membrane stresses would not be strong enough to hold the entire stream back. In Figure 9b for the triple-valued case, when λ is larger (and the margins therefore thinner), it is the basal stress that acts to stop runaway of the ice stream. In contrast, in the double-valued case there is a constant, very low resistance provided by the bed underneath the stream, and so resistance in the margins must be larger for the ice stream to be in balance.

Figure 9f is a plot of the magnitude of the lateral shear stress throughout the stream. As λ increases, the lateral shear magnitude also increases, due to the larger velocity change occurring over the margin. There is insufficient basal traction to support the stream, so membrane stresses play a more significant role in balancing the driving stress.

In summary, under a triple-valued sliding law, at lower values of λ the lateral shear and the basal drag both play an important role in the force balance of an ice stream; while at higher values the basal stress plays the dominant role in providing the resistive drag. A double-valued sliding law, however, enforces a low basal stress beneath the ice stream and so a restricted range of parameters is allowed, such that membrane stresses are large enough to hold back the ice stream throughout. For the membrane stresses to be large enough at higher values of λ , a larger velocity difference across the ice-stream margins is required (hence larger values of $\partial u_b / \partial y$).

5.2. A suitable value of λ ?

Throughout this work we have presented models with various values of λ to explore the controls on stress balances in ice streams. How does the scale, λ , affect the proportion of velocity which is due to sliding both inside and outside an ice stream? Figure 10a is a plot showing the fraction of the ice-stream velocity that is due to sliding at the bed; Figure 10b illustrates the fraction of surface velocity due to sliding at the bed over the entire domain for various values of λ in both the Newtonian and non-Newtonian cases.

In the ice stream itself, increasing λ results in a smaller proportion of the streamflow due to sliding, since vertical shear is favoured in the stress balance. For $\lambda \sim \mathcal{O}(10^{-2})$, over 99% of the flow in the stream is due to sliding, as has been observed in some Antarctic ice streams (e.g. Lüthi, 2010).

The triple-valued sliding law predefines the basal velocity both within and outside the ice stream. In particular, the sliding velocity outside the stream corresponds to the point where the slow stable branch intersects, $\tau_b = \tau_d = 1$ in Figure 1. The high proportion of velocity outside the stream due to sliding for small λ is a consequence of this; the vertical shear adds only a very small proportion of velocity. If, however, there were no slip outside the ice stream (if the ice were frozen to the bed) then there would still be some flow, all due to vertical shearing, outside the ice stream. This is in contrast to the SSA, which would result in no flow.

A clear benefit, therefore, in using a hybrid formulation (such as the one described in this paper) is that it can attribute varying degrees of surface velocity to sliding at the bed over a single domain. The SSA produces vertically uniform, plug-flow solutions, which may be accurate in the ice stream itself but do not accurately represent the transition to slow flow outside the stream. The SSA also cannot be used to model the emergence of ice streams, since it provides an inaccurate description of the ice flow before the stream has developed. Of course, the SIA with added sliding also allows different areas of the bed to have varying ratios of surface velocity due to sliding (as in the high- λ limit in these plots), but it is well known that the SIA rapidly loses its accuracy as sliding increases (e.g. Gudmundsson, 2003). The SIA does not include membrane stresses in the stress balance which, as we have shown here, have important stabilizing effects on ice-stream formation.

The model formulation presented in this paper also has the potential to be applied to other regions of an ice sheet, where there are no abrupt changes in basal or surface elevation and the basal stress is non-zero (i.e. $\lambda \neq 0$ to avoid the membrane stress term in Eqn (5) becoming infinite). These are valid assumptions in the region of grounding zones, although not over the grounding line itself, where the transition to a shear-free model occurs.

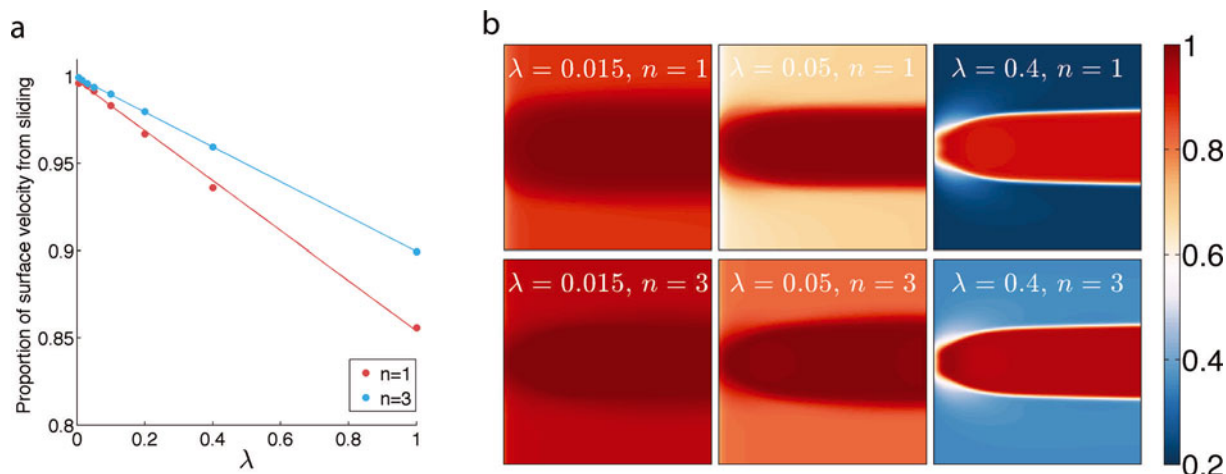


Fig. 10. Plots illustrating the fraction of surface velocity due to sliding at the bed under a triple-valued sliding law. In (a) the fraction within the ice stream is plotted with different values of λ for both Newtonian and non-Newtonian rheology. In (b) this value is plotted over the domain for specific cases.

The main advantage of this formulation, however, is the fact that it can accurately model ice that is sliding rapidly while also accrediting varying degrees of velocity to sliding over the domain; this is most useful in the region of ice streams where there are abrupt changes in the dominant motion.

5.3. Limitations of the model

The model used in this work is idealized so it is possible to identify critical controlling mechanisms associated with ice-stream stress balances, to improve our understanding of ice-stream stability.

An important limitation of the model is that we do not incorporate energy conservation, and so have assumed the ice to be at a constant temperature. It is well known, however, that thermal effects play an important role in ice-stream dynamics, since ice-stream beds have been found to be at melting point (Engelhardt and others, 1990; Iken and others, 1993). Moreover, Clarke and others (1977) suggested that streaming can be an inherent feature of ice sheets and glaciers under certain conditions, due to a creep instability from purely thermomechanical feedbacks. Further investigations including ice dynamics coupled with the thermodynamics used the SIA (MacAyeal, 1992; Payne, 1995; Payne and Dongelmans, 1997). Hindmarsh (2006a) then demonstrated that the inclusion of membrane stresses dampens these thermomechanical instabilities at short transverse wavelengths, although a thermoviscous feedback mechanism does still provide a mechanism for stream formation under the SSA and full Stokes. While our work to date has focused on feedbacks relating to the basal boundary condition, we intend to include thermal effects more comprehensively in future work. Including them in the rheology would have significant effects at the margins; we would expect the shear thinning effect to be further increased.

Another important aspect neglected in this work is the stabilizing effect of buttressing from ice shelves (e.g. Thomas, 1979; Hindmarsh, 2006b; Goldberg and others, 2009) and the corresponding destabilizing effect that calving events can have on an ice stream (e.g. Hughes, 1992). In this study we have cut off our domain before the grounding line and so include no ice-shelf/ice-sheet interaction. We would not, however, expect these effects to significantly alter our

results. The hybrid formulation would still provide an apt description of ice-sheet flow, and while buttressing might dampen instabilities (and similarly calving events might allow an instability to develop), this would only add some irregularity to results and some quantitative changes in the location of divides between flow regimes.

6. SUMMARY AND CONCLUSIONS

The theoretical model outlined in Section 2 introduces a new hybrid formulation suitable for describing ice-flow dynamics both in, and in the vicinity of, ice streams. The details of the derivation are provided in Appendix A. To benchmark the model we consider a set-up based on Sayag and Tziperman (2009) and apply a triple-valued sliding law at the bed. We show our results to be in agreement with theirs. We then look at the interplay of the triple-valued sliding law with the hybrid approximation, demonstrating the importance of using a model that includes both vertical shear and longitudinal stresses. Variations in the choice of the scaling parameter, λ , given a certain forcing, can alter the flow behaviour significantly. This value also governs shear margin width, as demonstrated with a simple scaling argument and by comparison of simulations with different values of λ . The hybrid approximation allows us to compare the significance of different stress components and study, in more detail, their relative importance in ice-stream formation.

We have also examined the effect of using a double-valued sliding law (Section 4). Simple physical considerations justify experimenting with a law of this form. While the triple-valued sliding law might represent behaviour due to switching between drainage systems (Sayag and Tziperman, 2009), or a thermoviscous feedback mechanism (Fowler and Johnson, 1995, 1996), its properties mean that there is only a small difference in basal stress inside and outside an ice stream (Fig. 9b). This is not the case under most ice streams, where the basal stress is considerably lower (e.g. Kamb, 2001; Joughin and others, 2004) and there is evidence that the till deforms with Coulomb-plastic behaviour (e.g. Iverson and others, 1998; Tulaczyk and others, 2000a; Kamb, 2001; Joughin and others, 2004; Schoof, 2004). We therefore experimented with a sliding law of the form of Eqn (21), that

specifies a low basal stress under fast-flowing ice. We found a scaling showing the critical dependence of the ice-stream velocity on the width of an ice stream, the basal yield stress of the underlying till, the bed slope and the parameters λ and ε for membrane stresses to be sufficient to balance the gravitational driving stress in an ice stream.

Our results demonstrate the benefits of using a hybrid of the SIA and SSA when describing ice flow in the region of ice streams. Varying the scaling parameter, λ , in the model results in behaviour variability given the same forcing; the stabilizing effects of membrane stresses become apparent at low values of the stress ratio, while at $\lambda \sim \mathcal{O}(1)$ the increased flux due to the vertical shear inhibits the formation of ice streams.

Having considered two heuristic sliding laws in this study, the results further suggest that there are many potential hydraulic mechanisms occurring under the ice that can give rise to ice streams and surging behaviour. Winsborrow and others (2010) describe seven potential controls on ice-stream location, all of which had been previously proposed in the literature, and suggest that topographic focusing, 'soft' subglacial geology, subglacial meltwater routing and calving margins are the most common controlling factors. The spatio-temporal dynamics of ice streams will vary, depending on which of these controlling factors are dominant, and so it is important to work more on understanding each of them, and interactions between them. Using purely phenomenological sliding laws allows us to gain qualitative insight into the effect of different controlling mechanisms. For example, in this work, different assumptions about drainage behaviour and till plasticity lead us to formulate sliding laws of the form of Eqns (8) and (21), and both result in characteristic streaming behaviour.

The results therefore emphasize the importance of continued research on the coupled dynamics of ice streams and subglacial hydrology. The parameter space of present models is large, and many of the parameters are unconstrained by observation. While work is already being done with plastic-bed and simplified hydrology models (e.g. Bueler and Brown, 2009; Bougamont and others, 2011; Van Pelt and Oerlemans, 2012), there is scope for further work in this area, not only considering plastic till behaviour. Furthermore, although using idealized models (such as considered in this paper) may not accurately represent all the complicated physical processes taking place at the bed, they do help to identify critical controlling mechanisms associated with the problem. Our aim for future work is therefore to represent the physics at the bed more directly, rather than through parameterized sliding laws, and to investigate the coupled behaviour in greater depth.

ACKNOWLEDGEMENTS

We thank the Oxford Supercomputing Centre for cluster-time and computing support, R. Sayag and J. Neufeld for useful discussion, and the reviewers for constructive reviews that helped us to improve the manuscript. This work was supported by the UK Natural Environment Research Council (NE/I528485/1). R.F.K. is supported by a Research Councils UK Academic Fellowship. A.C.F. acknowledges the support of the Mathematics Applications Consortium for Science and Industry (www.macs.iu.ie) funded by the Science Foundation Ireland mathematics initiative grant 06/MI/005.

REFERENCES

- Acheson DJ (1990) *Elementary fluid dynamics*. Oxford University Press, Oxford
- Alley RB, Blankenship DD, Bentley CR and Rooney ST (1986) Deformation of till beneath Ice Stream B, West Antarctica. *Nature*, **322**(6074), 57–59 (doi: 10.1038/322057a0)
- Alley RB, Blankenship DD, Bentley CR and Rooney ST (1987) Till beneath Ice Stream B. 3. Till deformation: evidence and implications. *J. Geophys. Res.*, **92**(B9), 8921–8929 (doi: 10.1029/JB092iB09p08921)
- Anandakrishnan S, Blankenship DD, Alley RB and Stoffa PL (1998) Influence of subglacial geology on the position of a West Antarctic ice stream from seismic observations. *Nature*, **394**(6688), 62–65 (doi: 10.1038/27889)
- Balay S, Gropp WD, McInnes LC and Smith BF (1997) Efficient management of parallelism in object-oriented numerical software libraries. In Arge E, Bruaset AM and Langtaten HP eds. *Modern software tools for scientific computing*. Birkhäuser Boston, Cambridge, MA
- Balay S and 8 others (2012a) *PETSc users manual*. (Tech. Rep. ANL-95/11, Rev. 3.3) Argonne National Laboratory, Argonne, IL
- Balay S and 7 others (2012b) PETSc. <http://www.mcs.anl.gov/petsc/>
- Bamber JL, Vaughan DG and Joughin I (2000) Widespread complex flow in the interior of the Antarctic ice sheet. *Science*, **287**(5456), 1248–1250 (doi: 10.1126/science.287.5456.1248)
- Bell RE and 6 others (1998) Influence of subglacial geology on the onset of a West Antarctic ice stream from aerogeophysical observations. *Nature*, **394**(6688), 58–62 (doi: 10.1038/27883)
- Bennett MR (2003) Ice streams as the arteries of an ice sheet: their mechanics, stability and significance. *Earth-Sci. Rev.*, **61**(3–4), 309–339 (doi: 10.1016/S0012-8252(02)00130-7)
- Bindschadler R, Chen X and Vornberger P (2000) The onset area of Ice Stream D, West Antarctica. *J. Glaciol.*, **46**(152), 95–101 (doi: 10.3189/172756500781833377)
- Bindschadler R, Bamber J and Anandakrishnan S (2001) Onset of streaming flow in the Siple Coast region, West Antarctica. In Alley RB and Bindschadler RA eds. *The West Antarctic ice sheet: behavior and environment*. American Geophysical Union, Washington, DC, 123–136
- Blankenship DD, Bentley CR, Rooney ST and Alley RB (1986) Seismic measurements reveal a saturated porous layer beneath an active Antarctic ice stream. *Nature*, **322**(6074), 54–57 (doi: 10.1038/322054a0)
- Blatter H (1995) Velocity and stress fields in grounded glaciers: a simple algorithm for including deviatoric stress gradients. *J. Glaciol.*, **41**(138), 333–344
- Bougamont M, Price S, Christoffersen P and Payne AJ (2011) Dynamic patterns of ice stream flow in a 3-D higher-order ice sheet model with plastic bed and simplified hydrology. *J. Geophys. Res.*, **116**(F4), F04018 (doi: 10.1029/2011JF002025)
- Bueler E and Brown J (2009) Shallow shelf approximation as a 'sliding law' in a thermomechanically coupled ice sheet model. *J. Geophys. Res.*, **114**(F3), F03008 (doi: 10.1029/2008JF001179)
- Clarke GKC (2005) Subglacial processes. *Annu. Rev. Earth Planet. Sci.*, **33**, 247–276 (doi: 10.1146/annurev.earth.33.092203.122621)
- Clarke GKC, Nitsan U and Paterson WSB (1977) Strain heating and creep instability in glaciers and ice sheets. *Rev. Geophys. Space Phys.*, **15**(2), 235–247
- Clarke TS and Echelmeyer K (1996) Seismic-reflection evidence for a deep subglacial trough beneath Jakobshavns Isbræ, West Greenland. *J. Glaciol.*, **43**(141), 219–232
- Doake CSM and 7 others (2001) Rutford Ice Stream, Antarctica. In Alley RB and Bindschadler RA eds. *The West Antarctic ice sheet: behavior and environment*. American Geophysical Union, Washington, DC, 221–235
- Echelmeyer KA, Harrison WD, Larsen C and Mitchell JE (1994) The role of the margins in the dynamics of an active ice stream. *J. Glaciol.*, **40**(136), 527–538

- Engelhardt H and Kamb B (1991) Antarctic Ice Stream B: conditions controlling its motion and interactions with the climate system. *IAHS Publ.* 208 (Symposium at St Petersburg 1990 – *Glaciers–Ocean–Atmosphere Interactions*), 145–154
- Engelhardt H, Humphrey N, Kamb B and Fahnestock M (1990) Physical conditions at the base of a fast moving Antarctic ice stream. *Science*, **248**(4951), 57–59 (doi: 10.1126/science.248.4951.57)
- Fountain AG and Walder JS (1998) Water flow through temperate glaciers. *Rev. Geophys.*, **36**(3), 299–328 (doi: 10.1029/97RG03579)
- Fowler AC (1981) A theoretical treatment of the sliding of glaciers in the absence of cavitation. *Philos. Trans. R. Soc. London, Ser. A*, **298**(1445), 637–681 (doi: 10.1098/rsta.1981.0003)
- Fowler AC (1987a) Sliding with cavity formation. *J. Glaciol.*, **33**(115), 255–267
- Fowler AC (1987b) A theory of glacier surges. *J. Geophys. Res.*, **92**(B9), 9111–9120
- Fowler AC (1997) *Mathematical models in the applied sciences*. Cambridge University Press, Cambridge
- Fowler AC (2010) Weertman, Lliboutry and the development of sliding theory. *J. Glaciol.*, **56**(200), 965–972
- Fowler AC (2011) *Mathematical geoscience*. Springer, London
- Fowler AC and Johnson C (1995) Hydraulic run-away: a mechanism for thermally regulated surges of ice sheets. *J. Glaciol.*, **41**(139), 554–561
- Fowler AC and Johnson C (1996) Ice-sheet surging and ice-stream formation. *Ann. Glaciol.*, **23**, 68–73
- Fowler AC and Larson DA (1978) On the flow of polythermal glaciers. I: Model and preliminary analysis. *Proc. R. Soc. London, Ser. A*, **363**(1713), 217–242
- Goldberg DN (2011) A variationally derived, depth-integrated approximation to a higher-order glaciological flow model. *J. Glaciol.*, **57**(201), 157–170 (doi: 10.3189/002214311795306763)
- Goldberg DN, Holland DM and Schoof CG (2009) Grounding line movement and ice shelf buttressing in marine ice sheets. *J. Geophys. Res.*, **114**(F4), F04026 (doi: 10.1029/2008JF001227)
- Gudmundsson GH (2003) Transmission of basal variability to a glacier surface. *J. Geophys. Res.*, **108**(B5), 2253 (doi: 10.1029/2002JB0022107)
- Hewitt IJ (2011) Modelling distributed and channelized subglacial drainage: the spacing of channels. *J. Glaciol.*, **57**(202), 302–314 (doi: 10.3189/002214311796405951)
- Hindmarsh RCA (2004) A numerical comparison of approximations to the Stokes equations used in ice sheet and glacier modeling. *J. Geophys. Res.*, **109**(F1), F01012 (doi: 10.1029/2003JF000065)
- Hindmarsh RCA (2006a) Stress gradient damping of thermoviscous ice flow instabilities. *J. Geophys. Res.*, **111**(B12), B12409 (doi: 10.1029/2005JB004019)
- Hindmarsh RCA (2006b) The role of membrane-like stresses in determining the stability and sensitivity of the Antarctic Ice Sheets: back pressure and grounding line motion. *Philos. Trans. R. Soc. London, Ser. A*, **364**(1844), 1733–1767 (doi: 10.1098/rsta.2006.1797)
- Hindmarsh RCA (2012) An observationally validated theory of viscous flow dynamics at the ice-shelf calving front. *J. Glaciol.*, **58**(208), 375–387 (doi: 10.3189/2012JoG11J206)
- Hindmarsh RCA and Payne AJ (1996) Time-step limits for stable solutions of the ice-sheet equation. *Ann. Glaciol.*, **23**, 74–85
- Hughes T (1992) On the pulling power of ice streams. *J. Glaciol.*, **38**(128), 125–151
- Hulbe CL and MacAyeal DR (1999) A new numerical model of coupled inland ice sheet, ice stream, and ice shelf flow and its application to the West Antarctic Ice Sheet. *J. Geophys. Res.*, **104**(B11), 25 349–25 366 (doi: 10.1029/1999JB900264)
- Hulbe CL and Payne AJ (2001) The contribution of numerical modelling to our understanding of the West Antarctic ice sheet. In Alley RB and Bindschadler RA eds. *The West Antarctic ice sheet: behavior and environment*. American Geophysical Union, Washington, DC, 201–219
- Hutter K (1982) Dynamics of glaciers and large ice masses. *Annu. Rev. Fluid Mech.*, **14**, 87–130 (doi: 10.1146/annurev.fl.14.010182.000511)
- Hutter K (1983) *Theoretical glaciology; material science of ice and the mechanics of glaciers and ice sheets*. D. Reidel, Dordrecht/Terra Scientific, Tokyo
- Iken A and Bindschadler RA (1986) Combined measurements of subglacial water pressure and surface velocity of Findelengletscher, Switzerland: conclusions about drainage system and sliding mechanism. *J. Glaciol.*, **32**(110), 101–119
- Iken A, Echelmeyer K, Harrison W and Funk M (1993) Mechanisms of fast flow in Jakobshavn Isbræ, West Greenland: Part I. Measurements of temperature and water level in deep boreholes. *J. Glaciol.*, **39**(131), 15–25
- Iverson NR, Hooyer TS and Baker RW (1998) Ring-shear studies of till deformation: Coulomb-plastic behavior and distributed strain in glacier beds. *J. Glaciol.*, **44**(148), 634–642
- Jackson M and Kamb B (1997) The marginal shear stress of Ice Stream B, West Antarctica. *J. Glaciol.*, **43**(145), 415–426
- Joughin I and Tulaczyk S (2002) Positive mass balance of the Ross ice streams, West Antarctica. *Science*, **295**(5554), 476–480 (doi: 10.1126/science.1066875)
- Joughin I, MacAyeal DR and Tulaczyk S (2004) Basal shear stress of the Ross ice streams from control method inversions. *J. Geophys. Res.*, **109**(B9), B09405 (doi: 10.1029/2003JB002960)
- Kamb B (1987) Glacier surge mechanism based on linked cavity configuration of the basal water conduit system. *J. Geophys. Res.*, **92**(B9), 9083–9100 (doi: 10.1029/JB092iB09p09083)
- Kamb B (2001) Basal zone of the West Antarctic ice streams and its role in lubrication of their rapid motion. In Alley RB and Bindschadler RA eds. *The West Antarctic ice sheet: behavior and environment*. American Geophysical Union, Washington, DC, 157–199
- Kamb B and 7 others (1985) Glacier surge mechanism: 1982–1983 surge of Variegated Glacier, Alaska. *Science*, **227**(4686), 469–479
- Lemke P and 10 others (2007) Observations: changes in snow, ice and frozen ground. In Solomon S and 7 others eds. *Climate change 2007: the physical science basis. Contribution of Working Group I to the Fourth Assessment Report of the Intergovernmental Panel on Climate Change*. Cambridge University Press, Cambridge, 339–383
- Lliboutry L (1968) General theory of subglacial cavitation and sliding of temperate glaciers. *J. Glaciol.*, **7**(49), 21–58
- Lüthi MP (2010) Glaciology: Greenland's glacial basics. *Nature*, **468**(7325), 776–777 (doi: 10.1038/468776a)
- MacAyeal DR (1989) Large-scale ice flow over a viscous basal sediment: theory and application to Ice Stream B, Antarctica. *J. Geophys. Res.*, **94**(B4), 4071–4087 (doi: 10.1029/JB094iB04p04071)
- MacAyeal DR (1992) Irregular oscillations of the West Antarctic ice sheet. *Nature*, **359**(6390), 29–32 (doi: 10.1038/359029a0)
- McMeeking RM and Johnson RE (1986) On the mechanics of surging glaciers. *J. Glaciol.*, **32**(110), 120–132
- Morland LW and Johnson IR (1980) Steady motion of ice sheets. *J. Glaciol.*, **25**(92), 229–246
- Papanastasiou TC, Malamataris N and Ellwood K (1992) A new outflow boundary condition. *Int. J. Num. Meth. Fluids*, **14**(5), 587–608 (doi: 10.1002/fld.1650140506)
- Paterson WSB (1994) *The physics of glaciers*, 3rd edn. Elsevier, Oxford
- Payne AJ (1995) Limit cycles in the basal thermal regime of ice sheets. *J. Geophys. Res.*, **100**(B3), 4249–4263 (doi: 10.1029/94JB02778)
- Payne AJ and Dongelmans PW (1997) Self-organization in the thermomechanical flow of ice sheets. *J. Geophys. Res.*, **102**(B6), 12 219–12 233 (doi: 10.1029/97JB00513)
- Raymond C (1996) Shear margins in glaciers and ice sheets. *J. Glaciol.*, **42**(140), 90–102

- Raymond CF, Echelmeyer KA, Whillans IM and Doake CSM (2001) Ice stream shear margins. In Alley RB and Bindschadler RA eds. *The West Antarctic ice sheet: behavior and environment*. American Geophysical Union, Washington, DC, 137–155
- Rignot E, Mouginot J and Scheuchl B (2011) Ice flow of the Antarctic Ice Sheet. *Science*, **333**(6048), 1427–1430 (doi: 10.1126/science.1208336)
- Ritz C, Rommelaere V and Dumas C (2001) Modeling the evolution of Antarctic ice sheet over the last 420 000 years: implications for altitude changes in the Vostok region. *J. Geophys. Res.*, **106**(D23), 31 943–31 964 (doi: 10.1029/2001JD900232)
- Rommelaere V and Ritz C (1996) A thermomechanical model of ice-shelf flow. *Ann. Glaciol.*, **23**, 13–20
- Röthlisberger H (1972) Water pressure in intra- and subglacial channels. *J. Glaciol.*, **11**(62), 177–203
- Sayag R and Tziperman E (2008) Spontaneous generation of pure ice streams via flow instability: role of longitudinal shear stresses and subglacial till. *J. Geophys. Res.*, **113**(B5), B05411 (doi: 10.1029/2007JB005228)
- Sayag R and Tziperman E (2009) Spatiotemporal dynamics of ice streams due to a triple-valued sliding law. *J. Fluid Mech.*, **640**, 483–505 (doi: 10.1017/S0022112009991406)
- Sayag R and Tziperman E (2011) Interaction and variability of ice streams under a triple-valued sliding law and non-Newtonian rheology. *J. Geophys. Res.*, **116**(F1), F01009 (doi: 10.1029/2010JF001839)
- Schoof C (2004) On the mechanics of ice-stream shear margins. *J. Glaciol.*, **50**(169), 208–218
- Schoof C (2006) A variational approach to ice stream flow. *J. Fluid Mech.*, **556**, 227–251 (doi: 10.1017/S0022112006009591)
- Schoof C (2010) Ice-sheet acceleration driven by melt supply variability. *Nature*, **468**(7325), 803–806 (doi: 10.1038/nature09618)
- Schoof C (2012) Thermally driven migration of ice-stream shear margins. *J. Fluid Mech.*, **712**, 552–578 (doi: 10.1017/jfm.2012.438)
- Schoof C and Hindmarsh RCA (2010) Thin-film flows with wall slip: an asymptotic analysis of higher order glacier flow models. *Q. J. Mech. Appl. Math.*, **63**(1), 73–114 (doi: 10.1093/qjmam/hbp025)
- Shabtaie S and Bentley CR (1987) West Antarctic ice streams draining into the Ross Ice Shelf: configuration and mass balance. *J. Geophys. Res.*, **92**(B2), 1311–1336 (doi: 10.1029/JB092iB02p01311)
- Swithinbank CWM (1954) Ice streams. *Polar Rec.*, **7**(48), 185–186 (doi: 10.1017/S0032247400043746)
- Thomas RH (1979) The dynamics of marine ice sheets. *J. Glaciol.*, **24**(90), 167–177
- Truffer M and Echelmeyer KA (2003) Of isbræ and ice streams. *Ann. Glaciol.*, **36**, 66–72 (doi: 10.3189/172756403781816347)
- Truffer M, Echelmeyer KA and Harrison WD (2001) Implications of till deformation on glacier dynamics. *J. Glaciol.*, **47**(156), 123–134 (doi: 10.3189/172756501781832449)
- Tulaczyk SM, Kamb B and Engelhardt HF (2000a) Basal mechanics of Ice Stream B, West Antarctica. I. Till mechanics. *J. Geophys. Res.*, **105**(B1), 463–481 (doi: 10.1029/1999JB900329)
- Tulaczyk SM, Kamb B and Engelhardt HF (2000b) Basal mechanics of Ice Stream B, West Antarctica. II. Undrained-plastic-bed model. *J. Geophys. Res.*, **105**(B1), 483–494 (doi: 10.1029/1999JB900328)
- Van der Veen CJ (1999) *Fundamentals of glacier dynamics*. AA Balkema, Rotterdam
- Van Pelt WJJ and Oerlemans J (2012) Numerical simulations of cyclic behaviour in the Parallel Ice Sheet Model (PISM). *J. Glaciol.*, **58**(208), 347–360 (doi: 10.3189/2012JoG11J217)
- Walder JS (1986) Hydraulics of subglacial cavities. *J. Glaciol.*, **43**(112), 439–445
- Weertman J (1972) General theory of water flow at the base of a glacier or ice sheet. *Rev. Geophys. Space Phys.*, **10**(1), 287–333
- Weis M, Greve R and Hutter K (1999) Theory of shallow ice shelves. *Contin. Mech. Thermodyn.*, **11**(1), 15–50 (doi: 10.1007/s001610050102)
- Winkelmann R and 6 others (2011) The Potsdam Parallel Ice Sheet Model (PISM-PIK) – Part 1: Model description. *Cryosphere*, **5**(3), 715–726 (doi: 10.5194/tc-5-715-2011)
- Winsborrow MCM, Clark CD and Stokes CR (2010) What controls the location of ice streams? *Earth-Sci. Rev.*, **103**(1–2), 45–59 (doi: 10.1016/j.earscirev.2010.07.003)

APPENDIX A. MODEL DERIVATION

Dimensional force balance and mass conservation for slow viscous fluid flow are described by

$$\nabla \cdot \boldsymbol{\sigma} = -\mathbf{f}, \quad (\text{A1})$$

$$\nabla \cdot \mathbf{u} = 0, \quad (\text{A2})$$

where $\sigma_{ij} = -p\delta_{ij} + \tau_{ij}$ is the stress tensor and $\mathbf{f} = (0, 0, -\rho g)$ is the body force acting on the ice (p is pressure and τ_{ij} , u , ρ and g are defined in Table 1).

Taking p_a to be the atmospheric pressure, we apply a balance in normal stress (assuming no applied traction) at the ice surface,

$$\boldsymbol{\sigma} \cdot \mathbf{n}^s = -p_a \mathbf{n}^s, \quad (\text{A3})$$

assume zero normal velocity at the bed,

$$\mathbf{u} \cdot \mathbf{n}^b = 0, \quad (\text{A4})$$

and apply the surface kinematic boundary condition at the free surface (Acheson, 1990),

$$w(s) = \frac{\partial s}{\partial t} + \mathbf{u} \cdot \nabla s - a, \quad (\text{A5})$$

where $\mathbf{n}^s \propto (-\partial s/\partial x, -\partial s/\partial y, 1)$ and $\mathbf{n}^b \propto (\partial b/\partial x, \partial b/\partial y, -1)$ are the normals to the surface and bed, respectively.

We define the scales $[d]$, $[l]$, $[u]$, $[\eta]$, $[t]$, $[a]$ and $[\tau_b]$ as in Table 1. These scales are then used to non-dimensionalize Eqns (A1) and (A2), scaling the variables as $z = [d]z^*$, $x = [l]x^*$, etc. In terms of these dimensionless variables (dropping the * for simplicity), the individual components of the governing equations become

$$\frac{\partial \tau_{13}}{\partial z} = \frac{\partial p}{\partial x} - \frac{\varepsilon^2}{\lambda} \left(\frac{\partial \tau_{11}}{\partial x} + \frac{\partial \tau_{12}}{\partial y} \right), \quad (\text{A6})$$

$$\frac{\partial \tau_{23}}{\partial z} = \frac{\partial p}{\partial y} - \frac{\varepsilon^2}{\lambda} \left(\frac{\partial \tau_{12}}{\partial x} + \frac{\partial \tau_{22}}{\partial y} \right), \quad (\text{A7})$$

$$\frac{\partial p}{\partial z} = \frac{\varepsilon^2}{\lambda} \frac{\partial \tau_{33}}{\partial z} - 1, \quad (\text{A8})$$

$$0 = \frac{\partial u}{\partial x} + \frac{\partial v}{\partial y} + \frac{\partial w}{\partial z}, \quad (\text{A9})$$

having neglected terms of $\mathcal{O}(\varepsilon^2)$. We non-dimensionalize the boundary conditions similarly.

Integrating Eqn (A8) over z gives us an expression for the static pressure at depth z , which we substitute into Eqns (A6) and (A7). By rewriting τ_{33} as $\tau_{33} = -\tau_{11} - \tau_{22}$ and making the assumption that the ice surface does not change abruptly (i.e. we neglect $\frac{\partial}{\partial x}[\tau_{11}(s)\partial s/\partial x + \tau_{12}(s)\partial s/\partial y]$ and $\frac{\partial}{\partial y}[\tau_{11}(s)\partial s/\partial x + \tau_{12}(s)\partial s/\partial y]$) we are left with

$$\frac{\partial \tau_{13}}{\partial z} = \frac{\partial s}{\partial x} - \frac{\varepsilon^2}{\lambda} \left(2 \frac{\partial \tau_{11}}{\partial x} + \frac{\partial \tau_{12}}{\partial y} + \frac{\partial \tau_{22}}{\partial x} \right), \quad (\text{A10})$$

$$\frac{\partial \tau_{23}}{\partial z} = \frac{\partial s}{\partial y} - \frac{\varepsilon^2}{\lambda} \left(\frac{\partial \tau_{11}}{\partial y} + \frac{\partial \tau_{12}}{\partial x} + 2 \frac{\partial \tau_{22}}{\partial y} \right) \quad (\text{A11})$$

as the governing equations for the approximation.

The deformation of ice is usually modelled with a constitutive relation known as Glen’s flow law (Paterson, 1994),

$$\dot{\epsilon}_{ij} = A\tau^{n-1}\tau_{ij}, \tag{A12}$$

where $\dot{\epsilon}_{ij} = \frac{1}{2} \left(\frac{\partial u_i}{\partial x_j} + \frac{\partial u_j}{\partial x_i} \right)$ is the strain rate, A is a temperature-dependent rate factor and $\tau = \sqrt{\tau_{ij}\tau_{ij}}$.

The non-dimensional components of Glen’s law can be expressed as

$$\frac{\partial u}{\partial z} + \epsilon^2 \frac{\partial w}{\partial x} = \lambda A \tau^{n-1} \tau_{13}, \tag{A13}$$

$$\frac{\partial v}{\partial z} + \epsilon^2 \frac{\partial w}{\partial y} = \lambda A \tau^{n-1} \tau_{23}, \tag{A14}$$

$$\frac{\partial u}{\partial y} + \frac{\partial v}{\partial x} = A \tau^{n-1} \tau_{12}, \tag{A15}$$

$$2 \frac{\partial u}{\partial x} = A \tau^{n-1} \tau_{11}, \tag{A16}$$

$$2 \frac{\partial v}{\partial y} = A \tau^{n-1} \tau_{22}, \tag{A17}$$

$$2 \frac{\partial w}{\partial z} = A \tau^{n-1} \tau_{33}, \tag{A18}$$

where

$$\tau^2 = \tau_{13}^2 + \tau_{23}^2 + \frac{\epsilon^2}{\lambda^2} \left(\frac{1}{2} \tau_{11}^2 + \frac{1}{2} \tau_{22}^2 + \frac{1}{2} \tau_{33}^2 + \tau_{12}^2 \right). \tag{A19}$$

Initially we consider the limit, $\lambda \ll 1$. Equations (A13) and (A14) $\Rightarrow \partial u/\partial z, \partial v/\partial z \ll 1 \Rightarrow \mathbf{u} \approx \mathbf{u}_b$. We can therefore take \mathbf{u} as a function of x and y only. In turn, this implies that τ_{11}, τ_{12} and τ_{22} are also functions of just x and y .

We can hence integrate Eqns (A10) and (A11) with respect to z , and together with non-dimensional Eqns (A6) and (A7) we have

$$\boldsymbol{\tau}_s = -(s-z)\nabla s + \frac{\epsilon^2}{\lambda} \nabla \cdot ((s-z)\mathbf{S}), \tag{A20}$$

where $\boldsymbol{\tau}_s = (\tau_{13}, \tau_{23})$ and \mathbf{S} is the resistive stress tensor given by

$$\mathbf{S} = \boldsymbol{\tau} + \mathbf{I} \text{trace}(\boldsymbol{\tau}) = \begin{bmatrix} 2\tau_{11} + \tau_{22} & \tau_{12} \\ \tau_{12} & \tau_{11} + 2\tau_{22} \end{bmatrix}. \tag{A21}$$

Moreover, the same result is true for the case $\lambda \sim \mathcal{O}(1)$ when shearing is dominant. The terms of $\mathcal{O}(\epsilon^2/\lambda)$ are now very small ($\mathcal{O}(\epsilon^2)$) unless horizontal gradients of the longitudinal stresses ($\partial\tau_{11}/\partial x$, etc.) are very large, i.e. if the horizontal velocities, u, v , change very rapidly in space. In regions where such a rapid change is occurring, gradients in \mathbf{u} can be approximated by those of the sliding velocity, \mathbf{u}_b ; in regions where the sliding velocity is not changing rapidly the corrective terms are small. Hence the equations remain valid for all sliding regimes.

Since in this study we are considering an isothermal ice mass, we take the temperature-dependent rate factor in Glen’s flow law, A , to be a constant. Again making the assumption that the ice surface does not change abruptly, we can write Eqn (A20) as

$$(\tau_{13}, \tau_{23}) \approx (s-z)\boldsymbol{\gamma} \tag{A22}$$

where

$$\boldsymbol{\gamma} = -\nabla s + \frac{\epsilon^2}{\lambda} \nabla \cdot \mathbf{S}. \tag{A23}$$

Integrating the expression for mass conservation, Eqn (A9), over depth, with Eqns (A5) and (A4) as the

boundary conditions, we obtain

$$\frac{\partial h}{\partial t} + \nabla \cdot \mathbf{q} = a, \tag{A24}$$

where $\mathbf{q} = \int_b^s \mathbf{u} dz$ is the ice flux.

When $\lambda \ll 1$ this becomes

$$\frac{\partial h}{\partial t} + \nabla \cdot (h\mathbf{u}_b) = a. \tag{A25}$$

A correction only becomes significant when shear stresses play an important role in the ice motion, i.e. when sliding is small. In this case, Eqn (A19) becomes

$$\tau^2 \simeq \tau_{13}^2 + \tau_{23}^2 = (s-z)^2 |\boldsymbol{\gamma}|^2, \tag{A26}$$

and furthermore Eqns (A13) and (A14) $\Rightarrow (\tau_{13}, \tau_{23}) = \frac{1}{\lambda\tau^{n-1}} \left(\frac{\partial u}{\partial z}, \frac{\partial v}{\partial z} \right)$, giving

$$\frac{\partial \mathbf{u}}{\partial z} = \lambda\tau^{n-1}(s-z)\boldsymbol{\gamma} \approx -\lambda\tau^{n-1}(s-z)\nabla s, \tag{A27}$$

to $\mathcal{O}(\epsilon^2)$ accuracy.

Finally, substituting Eqn (A26) into Eqn (A27) and integrating over depth gives us the mass flux

$$\mathbf{q} = \int_b^s \mathbf{u} dz = h\mathbf{u}_b - \lambda \frac{h^{n+2}}{n+2} |\boldsymbol{\gamma}|^{n-1} \nabla s. \tag{A28}$$

We hence obtain the governing equations, as stated in Section 2.1:

$$\frac{\partial h}{\partial t} + \nabla \cdot \left(h\mathbf{u}_b - \lambda \frac{h^{n+2}}{n+2} |\boldsymbol{\gamma}|^{n-1} \nabla s \right) = a, \tag{A29}$$

$$\boldsymbol{\tau}_b = h\boldsymbol{\gamma}, \tag{A30}$$

where $\boldsymbol{\gamma}$ is given by Eqn (A23) with $\mathbf{u} = \mathbf{u}_b$. This is the most general form of the equations.

Note that since the $\mathcal{O}(\lambda)$ correction to \mathbf{q} in Eqn (A28) is only important when shear stresses are dominant ($\lambda \sim \mathcal{O}(1)$), $\tau^2 \simeq \tau_{13}^2 + \tau_{23}^2$ does not vary rapidly with x or y and so can be removed from inside the derivative in Eqn (A23) written out with the components of $\boldsymbol{\tau}_b$ substituted in from Glen’s flow law for \mathbf{S} . Furthermore, expanding $|\boldsymbol{\gamma}|^{n-1}$, retaining terms greater than $\mathcal{O}(\epsilon^2)$, shows that if $\lambda > \mathcal{O}(\epsilon^2)$, then $\boldsymbol{\gamma} = -\nabla s$ to $\mathcal{O}(\epsilon^2)$ accuracy.

We therefore have the simplification that in Eqn (A29), $\boldsymbol{\gamma}$ can be taken to be

$$\boldsymbol{\gamma} = \begin{cases} -\nabla s + \frac{\epsilon^2}{\lambda\tau^{n-1}} [\nabla^2 \mathbf{u}_b + 3\nabla(\nabla \cdot \mathbf{u}_b)] & \text{for all } \lambda \\ -\nabla s & \text{if } \lambda > \mathcal{O}(\epsilon^2) \end{cases} \tag{A31}$$

to $\mathcal{O}(\epsilon^2)$ accuracy.

Finally, by substituting the components of Glen’s law, Eqns (A13–A18), into Eqn (A19), together with expressions for $\partial u/\partial z$ and $\partial v/\partial z$ from Eqn (A27), we get

$$\begin{aligned} \tau^{2n} = & |\nabla s|^{2n} h^{2n} + \left(\frac{\epsilon}{\lambda} \right)^2 \left[2 \left(\frac{\partial u}{\partial x} \right)^2 + 2 \left(\frac{\partial v}{\partial y} \right)^2 \right. \\ & \left. + 2 \left(\frac{\partial u}{\partial x} \right) \left(\frac{\partial v}{\partial y} \right) + \left(\frac{\partial u}{\partial y} + \frac{\partial v}{\partial x} \right)^2 \right]. \end{aligned} \tag{A32}$$

Only in Eqn (A29) (Eqn (1) in main text) can we approximate τ^2 as $\tau_{13}^2 + \tau_{23}^2 = |\nabla s|^2 h$ in the expression for $\boldsymbol{\gamma}$. In equation (A30) (Eqn (5) in main text), the correction to $\boldsymbol{\gamma}$ is important in the limit of small λ and so the longitudinal stress terms cannot be neglected.

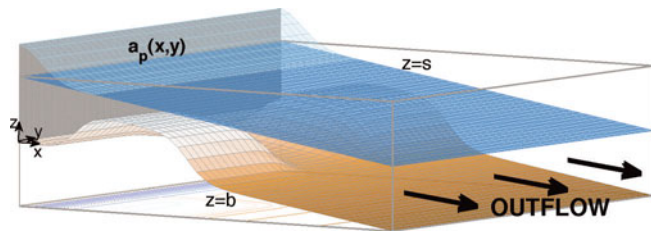


Fig. 11. Schematic illustrating the model set-up. There is zero inflow at the boundary, but instead an accumulation perturbation, $a_p(x, y)$, in the form of a Gaussian strip.

APPENDIX B. TEST SOLUTIONS FOR COMPARISON WITH NUMERICAL SOLUTION

We outline two steady-state analytic solutions as end-member cases that we use for comparison against the numerical solution. The first is for zero flow at the bed and the second is with the triple-valued sliding law applied at the bed (as Sayag and Tziperman, 2009).

B.1. SIA steady-state solution with zero sliding

We first consider the case when $\lambda = 1$ and there is no sliding at the bed ($\mathbf{u}_b = 0$). This gives us

$$\nabla \cdot \left(\frac{|\nabla s|^{n-1} h^{n+2}}{n+2} \nabla s \right) + a = 0, \tag{B1}$$

as for the non-dimensional SIA.

In the Newtonian case, on a flat bed and with boundary conditions $h = h_e$ at $x = 1$ and $h = h_s$ at $x = 0$, this has solution

$$h = [h_s^4 + (h_e^4 - h_s^4 + 6a)x - 6ax^2]^{\frac{1}{4}}, \tag{B2}$$

or, if we alternatively take the Neumann condition, $\partial h / \partial x = 0$, as the inflow condition, we have

$$h = [h_e^4 + 6a(1 - x^2)]^{\frac{1}{4}}. \tag{B3}$$

B.2. ‘Plug flow’ steady-state solution with the triple-valued sliding law

We consider the case where we have no flow variation in the y -direction and a constant depth field, i.e. we have $h(x, y) = 1$, $v(x, y) = 0$, $u(x, y) = u(x)$. The governing equations, Eqns (1) and (5), become

$$\frac{\partial u}{\partial x} = 0, \tag{B4}$$

$$\tau_{13}(b) = -\frac{\partial b}{\partial x} + 4\frac{\varepsilon^2}{\lambda} \frac{\partial^2 u_b}{\partial x^2}, \tag{B5}$$

$$\tau_{23}(b) = 0. \tag{B6}$$

With a triple-valued sliding law of the form

$$\tau_b = \frac{\mathbf{u}_b}{|\mathbf{u}_b|} \left[(|\mathbf{u}_b| - 1)^3 + \alpha(|\mathbf{u}_b| - 1) + 1 \right] \tanh(\beta|\mathbf{u}_b|), \tag{B7}$$

and following the analysis that Sayag and Tziperman (2009)

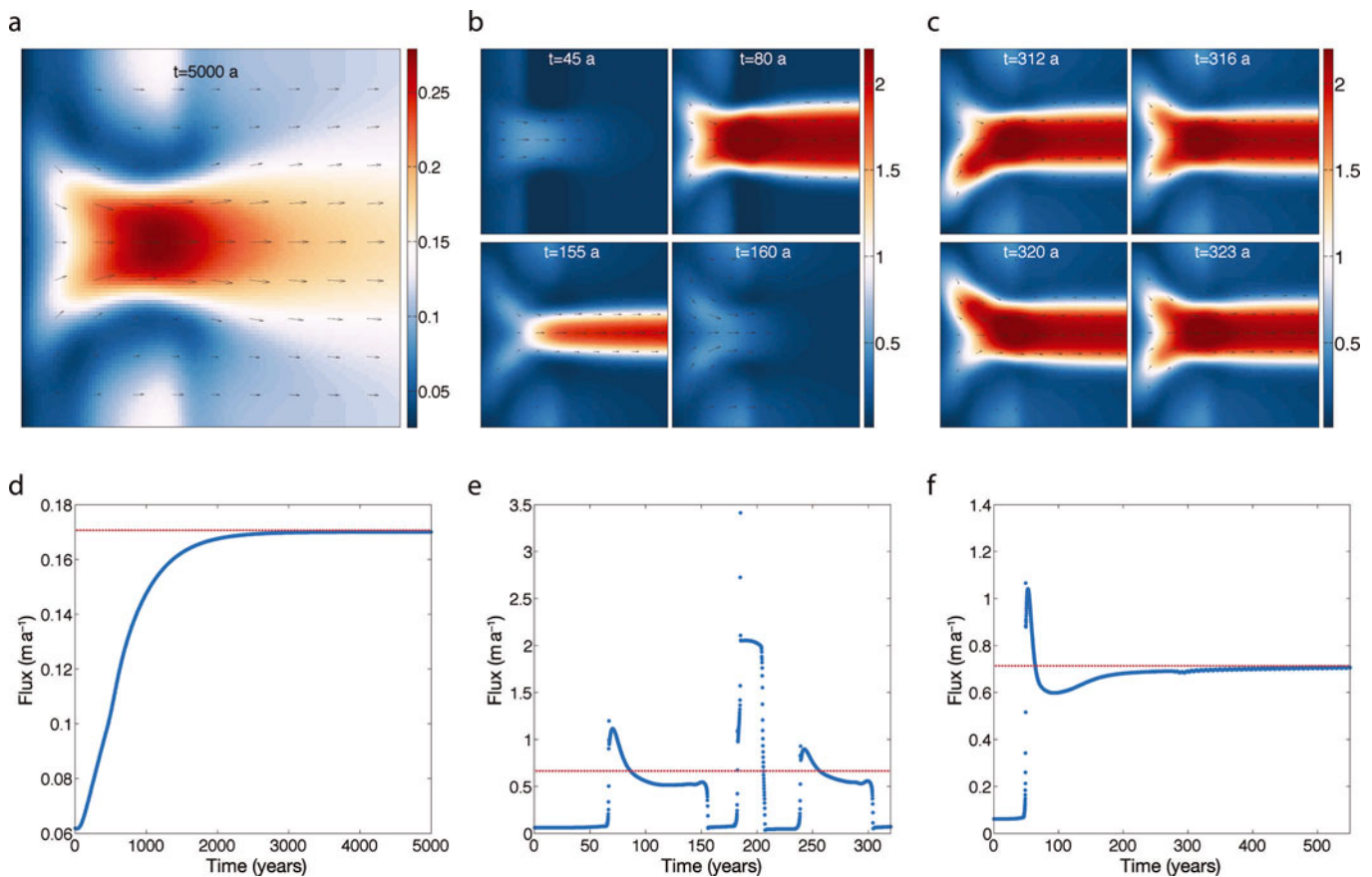


Fig. 12. Simulation results for three different incoming mass flux values (Gaussian strips of accumulation along the inflow boundary with magnitude 1 m a^{-1} , 7 m a^{-1} and 9 m a^{-1} for (a, d), (b, e) and (c, f), respectively). The plots in the top row are illustrations of the non-dimensional velocity fields, and the plots on the bottom row show time series of the total flux out of the solution domain (blue dots plotted at regular time intervals), with the total incoming flux also plotted (red dashed line).

carry out on this case, a solution exists of the form

$$u_b = 1 + (-\alpha^{-1/2}) \tanh \left[\left(-\frac{\alpha\lambda}{8\varepsilon^2} \right)^{1/2} (x - x_0) \right], \quad (\text{B8})$$

with $x_0 = (-8\varepsilon^2/\alpha\lambda)^{1/2} \tanh^{-1}(-\alpha^{-1/2})$.

APPENDIX C. ALTERNATIVE SET-UP

An alternative model set-up is with bedrock perturbations that channelize the flow in the onset region, as illustrated in Figure 11. We again enforce zero inflow to the domain and so apply an accumulation perturbation in a strip along $x = 0$, with a magnitude representing the sum of lesser

accumulations from upstream (as in Sayag and Tziperman, 2011). This results in the same three distinct flow regimes, but with less regularity to them as compared with the set-up used in the rest of the paper. Figure 12 illustrates results from a set of simulations. For the steady-state stream solution, there is an oscillation between which side of the domain 'feeds' the stream, an instability also seen by Sayag and Tziperman (2011) when they use a very similar model set-up. Benefits to this set-up include the fact that it is possibly more representative of the natural system, since pure ice streams often have prominent bedrock topography in their onset regions (Anandakrishnan and others, 1998; Bell and others, 1998).

MS received 31 July 2012 and accepted in revised form 12 January 2013